DOCTORAL THESIS

Alternative Energy Harvesting and Conversion Systems Based on Nanostructured Heterostructures

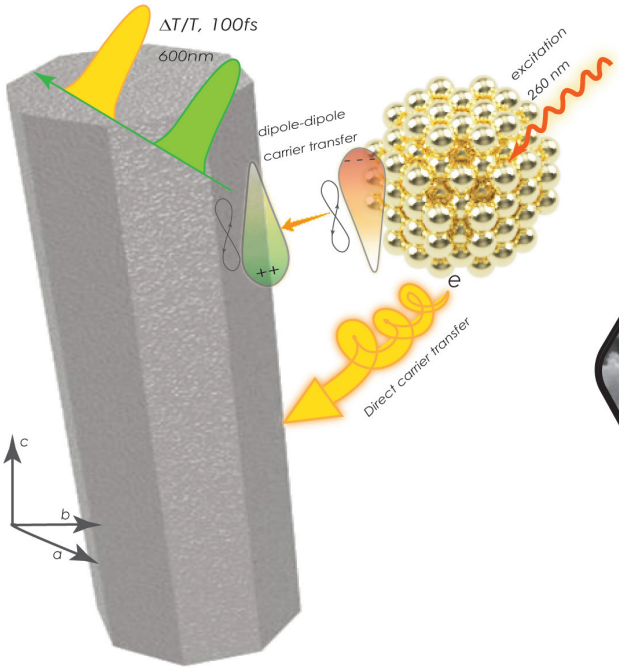

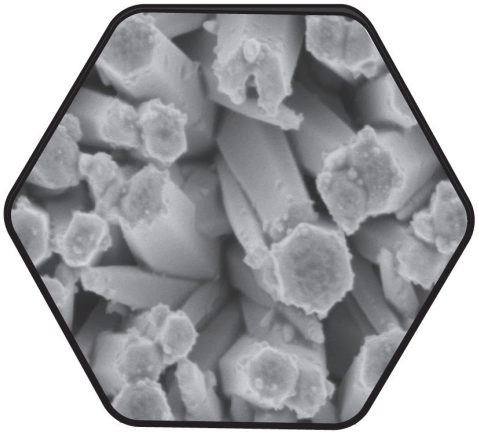

Mojtaba Gilzad Kohan

Experimental Physics

LULEÅ UNIVERSITY OF TECHNOLOGY

Alternative Energy Harvesting and Conversion Systems Based on Nanostructured Heterostructures

Mojtaba Gilzad Kohan

Doctoral Thesis

Experimental Physics

Department of Engineering Sciences and Mathematics

Luleå University of Technology

2021

To people I love

And

To people I lost

In the fell clutch of circumstance, I have not winced nor cried aloud.

Under the bludgeoning of chance my head is bloody, but unbowed.

William Ernest Henley

Abstract

Conversion and storage of the solar radiation into applicable forms of energy, using ubiquitous materials is of central importance that quests several disciplinary fields in both applied technology and fundamental science. Harnessing the solar energy received by the earth has the potential to replace the current sources of energy and it is imperative for sustainable development.

Since the early development of modern photovoltaics (PVs), based on silicon wafers, a rational step was the substantial development of the new generation PV technologies that can provide lower-cost and higher efficiency than their predecessors. Deliberate solutions involved employing different semiconducting materials that are indispensable, non-toxic and compatible with large-scale fabricating technologies.

Exploiting metal oxide (MOx) semiconductors, a broad class of non-toxic, cheap and abundant materials, is already promoted as a key component for high-performance optoelectronic devices and can be an ideal solution for inexpensive harnessing of sustainable energy resources like Sun light. The favorable band gap and high absorption cross-section of some MOx semiconductors permit utilizing different spectral region of the solar spectrum. However, at this present, the implication of MOx in high-throughput optoelectronic devices remained on the low side. Some of the main drawbacks that attain to poor performance of the MOx are associated with their poor intrinsic carrier mobility especially in p-type light absorbers and insufficient visible light absorption notably in n-type semiconductors.

The main aim of this thesis is to further contribute to the development and exploitation of this class of materials with the main focus on their role in optoelectronic devices and energy storage systems.

The content of this thesis considers two main aspect of the research.

Substantially, this work analyses the vital role of the interface engineering using nanostructured MOx, where we exploit unique phenomena such as intense electric field

confinement in 1dimensional (1D) structures resulting in ample light trapping in the fabricated heterojunctions. Unfortunately, this fact comes at the cost of introducing space charge region (SCR) limits in the fabricated devices attaining for poor derived currents.

Here I would probably spend couple of words for introducing the Co3O4 NR as the basis for p-n inverted nanorod junction…

Plasmonic metal nanoparticles (NPs) were conventionally used to extend the spectral response of the wide-bandgap semiconductors. Within the scheme of this thesis, we employ the silver plasmonic NPs in a 1D light harvesting structure of zinc oxide (ZnO), where we mediate hot-carrier collection of the charges via controlled illuminations.

Even further, we provide a comprehensive analysis on the hot-carrier redistribution mechanisms of the plasmonic NPs to semiconductor, providing direct experimental proof using transient pump-probe spectroscopy and time-resolved photoluminescence analysis. Our work resulted in a distinct understanding of the radiative and non-radiative carrier transfer between the active constituents of the system, which have not been corroborated previously.

In a parallel approach, the research activities in this work, take a few steps ahead and investigates the issues related to the disparities in the PV plants. A common prerequisite after conversion of the solar light using PV devices is the electrochemical storage of the energy where it can answer the needs for far-reaching energy requirements. Fostered by the intrinsic capacitance characteristic of the MOx, we interplay the role of the interfacial engineering in Co_3O_4 porous films and investigate the effect of their lateral architecture on Li+ ion adsorption and desorption properties.

Finally, our findings resulted in the fabrication of a hybrid device with dual functionality as an all-oxide PV system that can directly store the converted Sunlight as in a supercapacitor device. The prospect of this device can provide the over-potential required for direct storage of the converted solar energy into larger high storage systems.

In summary, the results presented in this thesis highlights the potential of the MOx semiconductors for photovoltaic and storage applications. We identify the various step-forward routes, which can provide the possibility of large-scale deployment of this novel class of materials.

Acknowledgements

This thesis is a brainchild of a man whose curiosity made him move forward, opening doors and leading him to new pathways. This journey would not have been possible without the valuable help of several incredibly thoughtful, supportive people whom I am thankful.

First of foremost, my deepest and sincere gratitude goes to my supervisor professor Alberto Vomiero. I am really happy that our way crossed-pathed and in debt of the opportunity provided by you which changed my life. An offering from the siege of the king is more than silver and gold. It is the seed of hope, a drop of faith of which the life will shape of.

I deeply thank my co-supervisor professor Isabella Concina, who she always consulted me like a friend both in science and life. I personally appreciate your dedication, keen interest, timely advice, meticulous scrutiny, scholarly instruction and scientific perspective.

There are certain people who make the world a better place, just by being in it. I deeply appreciate the sparkle that is in my life, Rosa Maria Pineda Huitron, for her support and several remarkable moments that cannot be forgotten and I leave the rest of my gratitude of her.

The daily battles won and the scientific moves forward could not be accomplished without the help of several friends and colleagues. To my dear friends and colleagues, Khabib Yusupov, Zhejian Cao (Jerry), Anton Landström, Pedram Ghamgosar, Dr, Federica Rigoni, and Tofik Ahmed Shifa (now professor). To the funniest officemate and a good friend Getachew Solomon. Special thanks to my friend Gustav Johansson for his help and proofreading of this thesis. To my dearest of people Marina Corvo Alguacil, for her endless support and patience, it was a pleasure getting to know you (well-deserving future Ph.D.). To my precious friend Stephanie Nunes for her immense wisdom and priceless friendship. I see nothing but a prosperous future for you. To Dr. Illia Dobryden for his friendly and fruitful conversations and his swift help with AFM characterizations. Special thanks to my friends in arms Johannes Strömbom, Johan Delissen, and Joakim Sandberg for their unconditional support and advices (sorry that I mess your names a lot).

I acknowledge all the people of the materials division, department of engineering sciences and mathematics, Luleå University of Technology for the very pleasant environment. Special thanks to Lars Frisk (the best of engineers) and Birgitta Lidström (the favorite administrator) for their instant support and great friendship.

In the prologue of which focused on the habit of showing gratitude, I recognize and acknowledge you the *reader*. The fruit of this thesis, from being a concept in my head to the present draft is a result of the last few years of my Ph.D. research. I hope it is a good guideline for your directions.

Especially to my family:

تقدیم به مادر و مشوق اصلی پیشرفت, تحصیل و زندگی ام فاطمه موفق مقدم. تقدیم به تمامی اعضای خانواده فایقه گیلزاد کهن, فایزه گیلزاد کهن و منا گیلزاد کهن. هرخط زندگی ام بی یاد شما بی معنی است.

Acronyms and Symbols

λ	Wavelength
Abs	Absorbance
AFM	Atomic force Microscopy
Ag	Silver
ALD	Atomic layer deposition
Al_2O_3	Aluminium oxide
Ar	Argon
AM	Atmospheric mass
CB	Conduction band
CE	Counter electrode
CO_2	Carbon dioxide
Co_3O_4	Tri cobalt tetra oxide
Cu_2O	Cuprous oxide
CVD	Chemical vapour deposition
DE	Defect emission
DSSC	Dye-sensitized solar cell
EDX	Energy dispersive X-ray spectroscopy
EQE	External quantum efficency
e^-	Electron
eV	Electron volt
Fe	Iron
Fe_3O_4	Tri iron tetra oxide (magnetite)
FF	Fill-factor
FTO	Fluorinated doped-tin oxide
He^{4+}	Helium ions
H_2O	Water

HR-TEM	High resolution transmission electron microscopy
J_{sc}	Short-circuit current density
MOx	Metal Oxide
MoO_3	Molybdenum trioxide
NBE	Near-band emission
NIR	Near infrared
NPs	Nanoparticles
NRs	Nanorods
NWs	Nanowires
PCE	Photo conversion efficency
PL	Photoluminescence
Pt	Platinum
PV	Photovoltaics
PVD	Physical vapor depositions
RBS	Rutherford backscattering
SC	Semiconductor
SSC	Solar supercapacitor
SEM	Scanning electron microscopy
TA	Transient absorption
TiO_2	Titanium dioxide
UV	Ultra violet
V_{oc}	Open-circuit potential
VA	Vertically aligned
VB	Valence band
Vis	Visible
XRD	X-ray diffraction pattern
ZnO	Zinc oxide
2D	2-dimensional

List of Articles

Article 1.

Vertically aligned Co_3O_4 nanorods as a platform for inverted all-oxide heterojunctions**,** M. Gilzad Kohan, G. Solomon, S. You, K. Yusupov, I. Concina and A. Vomiero, Nano Sel., 2021, nano.202000252 (featured as Additional Cover).

Article 2.

Optical Field Coupling in ZnO Nanorods Decorated with Silver Plasmonic Nanoparticles. Mojtaba Gilzad Kohan, Shujie You, Andrea Camellini, Isabella Concina, Margherita Zavelani Rossi, Alberto Vomiero J. Mater. Chem. C, minor rev. requested

Article 3.

In-depth Carrier Transport in a Barrier Variable Iron-oxide And Vertically Aligned Graphene Composite. Mojtaba Gilzad Kohan, Illia Dobryden, Daniel Forchheimer, Isabella Concina, Alberto Vomiero.

Article 4.

Plasma assisted vapor solid deposition of Co3O4 tapered nanorods for energy applications. M. Gilzad Kohan, R. Mazzaro, V. Morandi, S. You, I. Concina and A. Vomiero, J. Mater. Chem. A, 2019, 7, 26302–26310 (featured as Back Cover).

Article 5.

Direct solar conversion to energy storage; integrated solar supercapacitor. Mojtaba Gilzad Kohan, Isabella Concina, Antonia Infantes Molina, Alberto Vomiero,

Other Contributions

Articles in this section are not included in the context of this thesis.

I. ***Self-Powered Photodetectors Based on Core-Shell ZnO-Co_3O_4 Nanowire Heterojunctions,*** P. Ghamgosar, F. Rigoni, M. G. Kohan, S. You, E. A. Morales, R. Mazzaro, V. Morandi, N. Almqvist, I. Concina and A. Vomiero, ACS Appl. Mater. Interfaces, 2019, 11, 23454–23462.

II. ***ZnO-Cu_2O core-shell nanowires as stable and fast response photodetectors,*** P. Ghamgosar, F. Rigoni, S. You, I. Dobryden, M. G. Kohan, A. L. Pellegrino, I. Concina, N. Almqvist, G. Malandrino and A. Vomiero, Nano Energy, 2018, 51, 308–316.

III. ***Solar Cells and Light Management: Materials, Strategies and Sustainability***, M. Gilzad Kohan, I. Concina and A. Vomiero, in Elsevier, 2019, pp. 229–246, book chapter (Editors F. Enrichi and G. Righini).

IV. ***Semiconducting metal oxides empowered by graphene and its derivatives: Progresses and critical perspective on selected functional applications***, G. Solomon, M. G. Kohan, A. Landström, A. Vomiero and I. Concina, J. Appl. Phys., 2020, 128, 180905.

V. ***Fast Multifrequency Measurement of Nonlinear Conductance, R. Borgani,*** M. Gilzad Kohan, A. Vomiero and D. B. Haviland, Phys. Rev. Appl., 2019, 11, 044062.

VI. ***Au-Decorated Ce-Ti Mixed Oxides for Efficient CO Preferential Photooxidation,*** A. Infantes-Molina, A. Villanova, A. Talon, M. G. Kohan, A. Gradone, R. Mazzaro, V. Morandi, A. Vomiero and E. Moretti, ACS Appl. Mater. Interfaces, 2020, 12, 38019–38030.

VII. ***Resonance strengths in the N 14 (p,γ) O 15 astrophysical key reaction measured with activation,*** G. Gyürky, Z. Halász, G. G. Kiss, T. Szücs, A. Csík, Z. Török, R. Huszánk, M. G. Kohan, L. Wagner and Z. Fülöp, Phys. Rev. C, 2019, 100, 015805.

VIII. ***Decorating vertically aligned MoS_2 nanoflakes with silver nanoparticles for inducing a bifunctional electrocatalyst towards oxygen evolution and oxygen reduction reaction,*** G. Solomon, M. G. Kohan, M. Vagin, F. Rigoni, R. Mazzaro, M. M. Natile, S. You, V. Morandi, I. Concina and A. Vomiero, Nano Energy, 2021, 81, 105664.

List of figures

Table of contents

SYNOPSIS

CHAPTER 1

Introduction

The ever-increasing concerns regarding energy shortage, greenhouse related environmental deterioration, are some of the driving forces leading to a dramatic reshape in our society's energy policy. Up to day, the world's energy supply is largely based on exploitation of fossil fuels. However, the use of fossil fuels, a finite and un-sustainable source of energy, is resulting in distinctive environmental impacts. Specifically, consumption of the fossil fuels in its bases, can create several concerning aspects, from climate change, uneven economical allocations and limited availability, which severely increases due to the increments of the energy demands.

Reasonably, in the quest to reduce our reliance on fossil fuels and prevent their consequent environmental impacts, exploring the renewable and sustainable sources of energy is both necessary and imperative. Part of the industrial and scientific work has turned its attention to the exploitation of renewable sources of energy like Solar irradiation, that are now providing more than 19% of the global energy consumption[1,2].

Sunlight among renewable energy sources, is one of the most abundant and attainable. The average solar energy, received on earth in an hour is somewhat more than the world's population consumption guideline for over a year, a quantity exceeding our energy demands[3]. In that respect, different attempts were made for efficiently convert and store solar radiation, in the applicable forms of energy using various devices, which in turn, resulted in growth of different scientific scopes and considerable fields of research.

One of the promising technologies which can exploit the solar radiation for direct conversion into electricity, a widely applicable form of energy, is the photovoltaic (PV) systems. The word photovoltaic is a combination of the Greek word origin, 'photo' meaning light and the 'voltaic' that is the dimension to measure electric potential at given time point. PV system on its basis, is extremely interconnected to the development of the

quantum mechanics[4]. In this framework, the initial responses of the photovoltaics were required to be explained by the definition of the light particles (quanta), however the wave particle duality of solar illumination was also turned to be an explicit parameter.

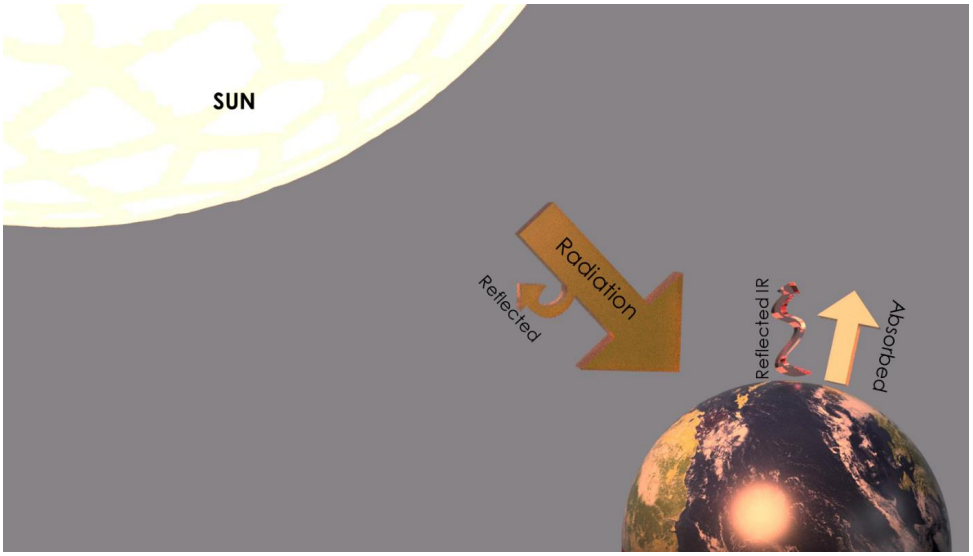

Figure 1: Schematic illustration of the solar energy, absorption, reflection and radiation.

The PV cells are conventionally fabricated using semiconductor materials, which act as insulators in dark due to lack of input energy (temperature, excitation, etc…) but as moderate conductors when energy is available[5]. In that regard, it was observed that certain semiconductors when excited by light can mobilize their carriers and generate electric current (Edmond Becquerel 1839)[6]. The basic principle of the PV system will be explained further in details in the next sections.

Silicon is the most dominant material for PV industry fulfilling the demands of the abundance and efficiency for the large scale fabrication. In that sense, commercial PV modules, which denote the first modern PVs fabricated in 1954, are based on silicon wafers, categorized as first generation solar cells. Parallel to the main dominance of the wafer based solar cells, the seek for the devices with the better photoconversion efficiency and subsequently cheaper manufacturing costs resulted in second and third generation PV devices, creating a boost in the alternative PV research.

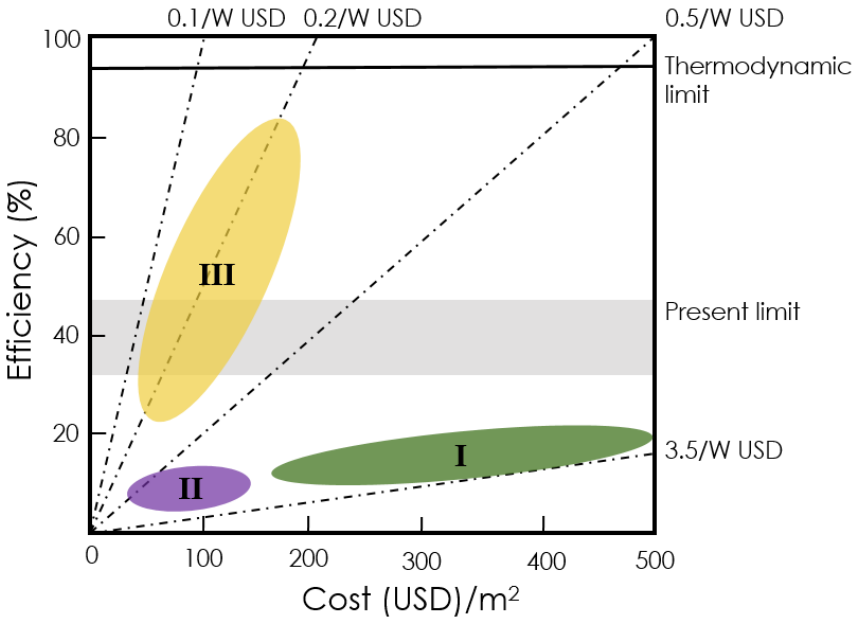

Figure 2: The criteria for the cost-efficiency evaluation of the different generation of photovoltaics[7]*. Updated from Solar cell efficiency tables (Version 58) June 2021, Green et al.* https://doi.org/10.1002/pip.3444 .

The ultimate goal of the *third generation* photovoltaics is to significantly increase device efficiencies whilst still using industrially scalable processes, abundant, cheap and non-toxic materials. In specific, the overview of the third generation PVs dictates a threefold landscape for large scale deployment. The overall foundation of the devices should consider the 25-years of life-time for the device design (**stability**) and rely on abundant and cheap manufacturing technologies such as roll-to-roll process and non-vacuum processing techniques (**scalability**). Crucially, the fabricated PV devices should be able to fulfil the terawatt challenge relative to their production cost (**efficiency**). Accordingly for renewable technologies covering 100% of the global energy demand in 2050, it is required for PV industry to adhere 25 TWp of the demand[8].

In this view, nanotechnology examines the practical point for the state-of-the-art development in the third generation PV devices. Low-dimensional geometries such as

nanostructured and thin film devices are the best candidate to decrease material usage, enhance light-matter interaction, and allow more efficient charge collection. As a key solution, nanotechnology can provide research approaches within the proper physical context related to PV performance enhancement and diversity of the energy harvesting technology.

In this thesis we approach to consider the three aforementioned important requirements for the bottom-up design of the investigated energy harvesting systems. An important focus of the conducted research will be drawn towards the fabrication and design of the metal-oxide (MOx) based heterojunction PVs, which forth fit the promising devices in the solar conversion technologies. MOx semiconductors, the main component of the MOx heterojunctions, on their basic nature are indispensable, low cost and stable material, which occasionally pose appropriate energy band-gap for active solar absorption. Consequently, MOx semiconductors drive an interesting framework for further research as a promising building blocks of future light harvesting systems. The explicit details on the fundamentals of MOx heterojunctions and the conducted research on them will be later discussed in this thesis.

1.1 STORAGE OF THE ENERGY; AN UNDENIABLE REQUIREMENT

Moving on to the realistic scenario of the sustainable energy resolution, the so far presented solar conversion technologies are concerned with the production of heat or electricity but, as considered as another important focus of the current work, a realistic energy transition without implementing innovative approaches for storage of the converted solar irradiation is rather impossible.

Electrochemical storage of the converted solar energy is one of the areas in which the PV systems can stabilize their output produced energy. Furthermore, they also find important applications where the solar grid in not present such as logistic, electrical vehicles, power electronics, etc.

It is rather a known fact that the solar PV systems are directly dependant to the received radiations in order to produce the reliable energy outputs. However, it is accounted for that solar radiation is rather intermittent phenomena and may inevitably vary depending

on the weather condition and day/night transition hours. In that sense, solar energy storage is the easiest method for dealing with the issues of *discontinuity* in PV systems. Consequently, it is fundamental to find the most appropriate energy storage device for particular applications and operational conditions.

Accordingly, the nature of the storage devices coupled with the PV systems can vary due to the criterion that the system is utilized and is operational. For instance the small power storage devices such as super-capacitors (SCs) are readily suitable for stabilizing the current output of the interconnected PVs, and provide fast-charge and discharge ability, although they are limited in providing high power densities. In contrary, the coupled PV systems with electrochemical energy storage devices such as batteries, is a common solution for large-scale PV facilities, providing high capacity of stored energy. However, it also results in some major charge-discharge losses and operational complexity.

1.2 DRIVES FOR RESEARCH IN THE ENERGY STORAGE SYSTEMS

The main requirement for nowadays energy storage systems, exerts to two major phenomena. (i) Fast **charging and discharging** of the energy storage systems whilst providing an efficient (ii) **power density** for long term use. In that sense, super capacitors (SCs) are an ideal solution for an intense charge and discharge operational condition, yet their unattainable short term power output hinders their major deployment. Unlike ordinary capacitors, of which minimizing the charge separation distance (dielectric thickness) and increasing the electrode area can correspond to higher capacitance values, in SCs charge separation is in order of nanometer scale at each electrodes interface (the solid-electrolyte interphase). Additionally, the central essence of SC design is based on physical adsorption and desorption of the ions, for fast charge and discharge processes, as opposed to battery cells that rely on chemical intercalation processes and Faradic reactions for charge storage. Certainly, such fundamentals, dictates the proper engineering of the employed electrodes used in SCs.

Correspondingly, nanotechnology provides an undeniable guideline to engineer the electrodes interface, designing appropriate surface area (porous structure, active crystalline facet selection, etc.), inherent permeable separating layers and even the

characteristic of the ionic medium. In the presented work we demonstrate the possibility of employing MOx semiconductors, which pose suitable capacitance values for ion adsorption processes through nanoscale interfacial engineering. Our work partially includes the design and analysis of the MOx based electrodes with 1dimensional (1D) nanostructures, their electrochemical characterization and their innovative optimal implications.

CHAPTER 2

Outline and approaches

The framework of this PhD thesis is to investigate two aspect of energy conversion and energy storage using innovative approaches and nanomaterials solely based on MOx semiconductors. The conducted research is mainly devoted to develop and optimize the photophysics of MOx semiconductors via different scientific methods, with scopes of fabricating new class of optoelectronic devices. In particular, we aim at answering next vivid questions with focus to improve the intrinsic shortcomings of MOx semiconductors in the areas of photovoltaics, photodetection and energy storage systems:

Solar light mediated energy conversion: light-energy conversion through environmentally friendly material and with facile processing technologies is of central importance for sustainable development. Can optoelectronic PV devices, based on MOx semiconductors, which pose environmental friendly and ambient stability, be designed so as to exploit the solar irradiation efficiently?

Nanostructuring an approach for light harvesting: the urge for development of the efficient light harvesting devices is normally quenched with intrinsic shortcomings of MOx light absorbers in carrier transport depth. Could it be possible to tailor the carrier transport properties of p-type light absorber MOx through their optimized nanostructuring?

Hot electron injection Yield: plasmonics have been widely used to passively increase the carrier transport in semiconductors and making devices more efficient by injecting the electrons that are not in thermal equilibrium into the system. However, the main hurdles in lack of efficiency of plasmonic devices are associated with the compatibility of the device architecture. Till what extend it is possible to optimize hot-electron harvesting architectures to significantly improve this process?

Extending the spectral range of MOx: the lack of sufficient light interaction in some common n-type MOx, such as zinc oxide (ZnO) and titanium dioxide (TiO_2) is a major drawback in their visible light driven applications. Plasmonics promote the possibility to

geometrically tune the spectral response of such semiconductors. Is it possible to design a scalable plasmonic device while catering for efficient and tunable photo-absorption?

Increasing the carrier penetration depth: a distinct issue in MOx light absorber materials is their low photoexcited carrier penetration depth. This fact corresponds to a competing trade-off in their light absorption cross-section versus the derived electrical current, making it difficult to design light harvesting MOx devices with considerable thicknesses exceeding tens of nanometer. Can we extend the carrier penetration depth of MOx semiconductors by designing hybrid systems using optically active functional materials?

Engineering the surface texture of MOx for energy storage: the functional MOx semiconductors can be applied in the energy storage systems such as SCs. The aspect of energy storage is highly related to the use of intrinsically high-capacitance materials and their nanoscale surface area morphology[9–11]. Can we alter the MOx electrodes surface area in order to optimize their ion adsorption and consequently their capacitive behavior?

Energy conversion and storage all at once: MOx semiconductors are some of the main building blocks of both energy conversion and energy storage systems. Is it possible to design a device with dual functionality that can directly convert and store the directed solar illumination?

Following the above mentioned research premises in the conducted work, the content of this thesis falls into the next categories:

- In chapter 3 we thoroughly introduce and explain some of the fundamental physical concepts behind the semiconducting materials in general and PV devices and SCs in particular. The conventional models for electrical properties of the PV systems and the SC devices will be explained briefly.
- In chapter 4 we introduce an all-oxide based heterojunction device which denotes the prospects of a promising PV device, based on thin-film architectures of ubiquitous n-type and p-type MOx semiconductors as active constituents of p-n junction.
- In Chapter 5 we delve into surface modification of MOx semiconductors using plasmonic nanoparticles (NPs) for solid-state visible light harvesting. We identify

some of the previously neglected radiative and non-radiative carrier transfer phenomena via implementing a thin passivating layer and advanced pump-probe spectroscopy.

- In chapter 6 we discuss the ample performance of the graphene and semiconductor junction. The role of the vertically aligned graphene scaffold in conjunction with the iron oxide (Fe_3O_4) light absorber for assisted in-depth photo-excited carrier transfer is comprehensively investigated.
- In chapter 7 we investigate the significance of employing nanostructured Co_3O_4 semiconductor with high intrinsic capacitance for energy storage SC applications. In addition, the prospect of storing converted solar illumination using a hybrid solar-SC device is thoroughly demonstrated by fabricating an innovative integrated device.
- In chapter 8 we discuss the potential road-map for MOx based optoelectronic devices, presenting the main opportunities and the most promising directions in the field.

CHAPTER 3

Background

This chapter is mainly devoted to explain some of the general concepts in the context of this thesis. It begins with an introduction to some of the already known relevant scientific backgrounds to the conducted work and concludes with some of the figures of merit for investigated optoelectronic devices of this thesis.

3.1. Semiconductors

Nowadays, PV research is heavily co-dependent to the semiconductor materials which are the main constituents of the PV devices and responsible for the conversion operations. The electronic structure of semiconductors are normally categorized as an intermediate state in between insulators and metals. If the material poses completely filled electronic bands and/or completely empty bands it will not contribute to electrical conductivity and such material is therefore an insulator. If the distance between the highest edge of the upper filled band (valence band) and the lower extreme of the empty allowed acceptor band (conduction band) is not too significant (e.g. 3.2 eV in ZnO) the material is called *semiconductor*. Such material is able to convey the carriers in its structure as a result of input energy such as light. In that sense, a small fraction of the electrons are available in the vicinity of the conduction band, leaving unoccupied states (holes) in the upper limits of their valence band. Metals are normally defined as materials with an overlap between their conduction and valence band making transport of the electrons in their bulk rather easy[12,13]. In Figure 3 the differences between metal, semiconductor and insulator band structure is shown schematically.

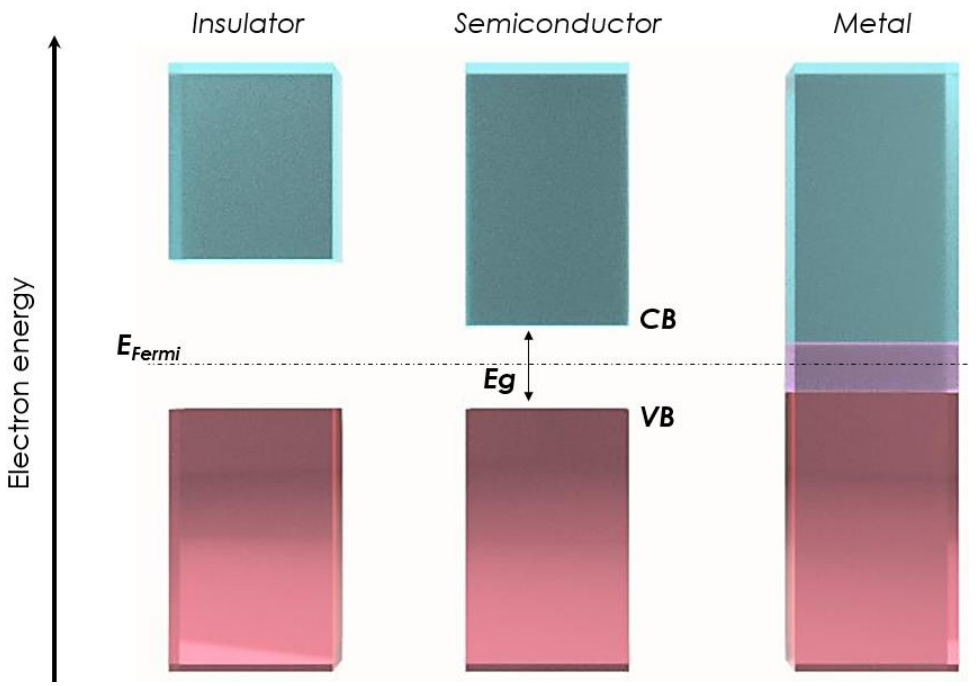

Figure 3: Energy band diagram for metal, semiconductor and insulator. For semiconductors and insulators the Fermi level lies between occupied valence band and unoccupied conduction band.

3.2. Photovoltaic effect

The early stage development of the modern PVs in 1950s (also known as the black cell), is vividly associated with a phenomena based on inhomogeneities in electronic band structure of the constituent semiconductors[14]. The main approach was based on introducing the electron donor (e.g. P, As, Sb) or acceptor (e.g. B, Al, Ga) elements to each stack of semiconductors, creating an *n*-type semiconductor (higher concentration of donor carriers) and *p*-type semiconductor (higher concentration of carrier acceptors). Interfacial junction of *p*-type and *n*-type semiconductors, also called *p*-*n* junction would give a rise to a rectified electronic transition from one side to another, called band bending[14]. The bending of the bands in the transition region has the effect that the acceptors (holes) in the *p* region are pushed below the Fermi level, i.e. the conduction band are occupied by the donors (electrons), whereas in *n* region donors are lifted above

Fermi level , i.e. valence band are unoccupied and thus positively charged (**Error! R eference source not found.**).

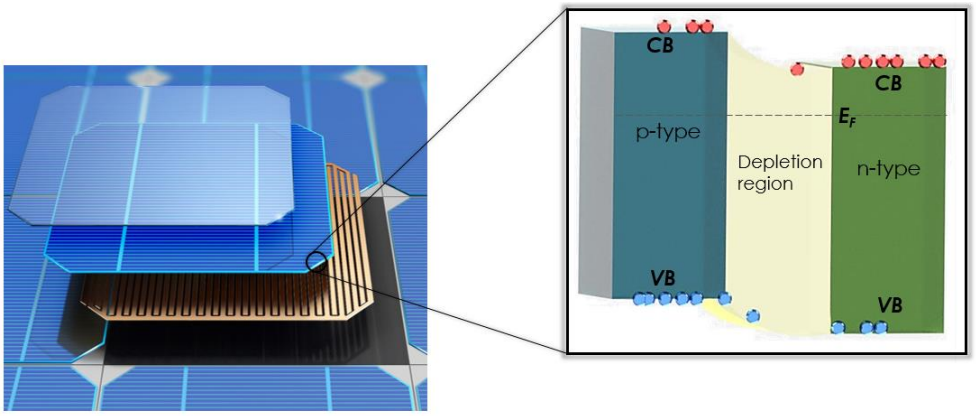

Figure 4: The energy band diagram of the electron-hole separation process in a conventional PV system.

Far outside of the depletion region, the electrons and holes are compensated by equally large electron and holes present in the bulk of semiconductors. These carriers are corresponded to the type of doping in the respective regions and they are denoted as *majority carriers*. Since the electrons and holes are able to mobilize freely, electrons can diffuse into *p*-type region and contrary holes into *n*-type region, where they are called *minority carriers*. In a thermal equilibrium and by considering the law of the mass action, the concentration of the majority carriers (electrons n_n and holes p_p) can be derived by:

$$n_n = N_{eff}^{C} \exp\left(-\frac{E_C^n - E_F}{kT}\right), \quad (1)$$

$$P_P = N_{eff}^{v} \exp\left(-\frac{E_F - E_V^P}{kT}\right), \quad (2)$$

Here, E_C^n and E_V^P are the energy levels for conduction and valence band edges of *n*-type and *p*-type semiconductor respectively. E_F is the Fermi level of materials and N_{eff}^{C} and N_{eff}^{v} are the effective density of states in Boltzmann statistics. The state of the carrier diffusion in a p-n junction as in Figure 4 (electrons diffusing from right to left and opposite direction for holes) is finally correspondent with an electric field E(x) and therefore a drift

current can be estimated for the junction. This electric current is the foundation of derived current in PVs, however different sources of loss should also be taken into account. In general, the ideal formulation for the output current (I) of the conventional PV devices is expressed as:

$$I = I_L - I_0(e^{qv/NkT} - 1) \quad (3)$$

Where I_L equals to the collected current in the absence of recombination in the bulk of semiconductor. I_0 is the reverse saturation current, N is the voltage dependent ideality factor and q is the effective carrier charge (4.78×10^{-21} c).

Such formulation can be used to determine the PV performance when non-radiative processes dominate the recombination. However, most of the approaches involve several different routes of radiative recombinations such as stimulated emissions when qV is close to band gap (E_g), or re-absorption or recycling of the trapped light[15] (The sources of recombination is quite diverse and severe in the PV field, here we avoid expressing different routes of recombinations based on cell design and semiconductor choice). These diverse choice of recombination routes can create several controversy on correctly determining the most robust PV design. However, it is rather liable to consider that most of the recombination approaches can be tackled using proper geometrical architectures and the material choice.

An interesting approach to solve the issues of predicting the derived current and the efficiency of the cell is to consider the behaviour of the PV devices by switching the attention on how the constituent active semiconductors behave with terrestrial light.

3.3. Shockley Queisser limit

The Shockley Queisser limit considers the fact that an efficient PV device would have to be an efficient absorber of solar flux and hence follow the similar radiation profile of the of the black-body emissions with compatible energy traits with semiconductor's band-gap[16]. By attributing the black-body radiation for energies level in line with semiconductor's bandgap and considering the possible band-to-band recombination, they were able to very simply calculate the net rate of recombination events occurring in the cell. Considering the ideality factor equal to 1 this limit leads instantly to the behaviour of ideal PV device:

$$I_0 = qA\left(\frac{2\pi kT}{h^3C^2}\right)\left[E_g^2 + 2(kT)E_g + 2(kT)^2\right]e^{-Eg/kT} \quad (4)$$

Where μ is the mobility of minority carriers of concentration, n and J is the current density perpendicular to the surface. E_g denotes the band gap of the material and corresponds to the Plank constant.

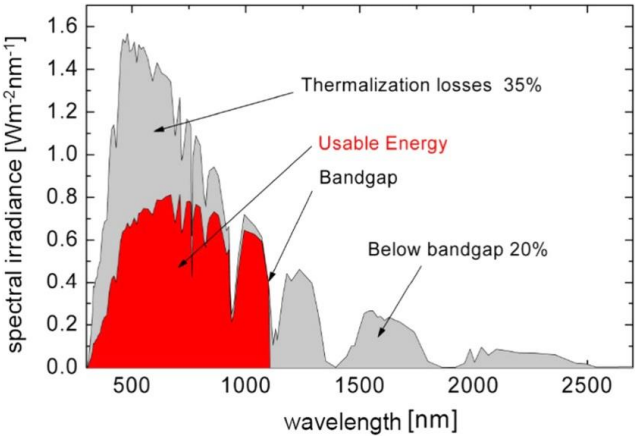

Figure 5: Spectral intensity distribution of solar flux spectrum as a function of wavelength at 6000 K[17].

The work of Shockley and Queisser represented a major conceptual advance and provided a new set of tools for analysing solar cell performance. However, a major drawback involves the fact that the model only considers the single absorber conventional devices and neglects some other type of conversion devices such as hot-carrier, tandem, etc[18].

The next section discusses the figures of merit in the energy storage systems with the main focus on the SCs devices. The inherent fast charge and discharging characteristics of SCs, and their remarkable capacitance values makes them a liable candidate for future road ahead of energy storage systems.

3.4. Supercapacitors

The basic operation nature of SCs present some major differences compared to conventional capacitors due to their fast charge–discharge rates, longer life cycle, higher output power, and enhanced energy density[19]. Generally SCs are categorized into two different groups. (i) The first group is based on double-layer electrical capacitor that stores

electrical energy as a result of electrostatic adhesions at the polarized electrode–electrolyte interface forming the double layer of charges. The charges are physically deposited by electrostatic attraction (physical adsorption), resulting in rapid charge–discharge kinetics, and longer life span (no chemical reaction is involved)[11]. Carbon materials such graphene, carbon nanotubes, graphite and activated carbon are mostly used as electrode materials for double-layer capacitors. (ii) The second group of SCs commonly referred to as a pseudocapacitor uses faradaic reactions to store electric energy where electronic transfer takes place without formation or breaking of any chemical bonding. RuO, Co_3O_4 and MnO are well-known pseudocapacitive materials with specific capacitance closer to their theoretical limit[20,21]. The electrochemical signature of pseudocapacitor materials is rather similar to the double-layer SCs, however they present higher energy densities as a result of drastically thicker ionic layer generated on their electrodes[22,23].

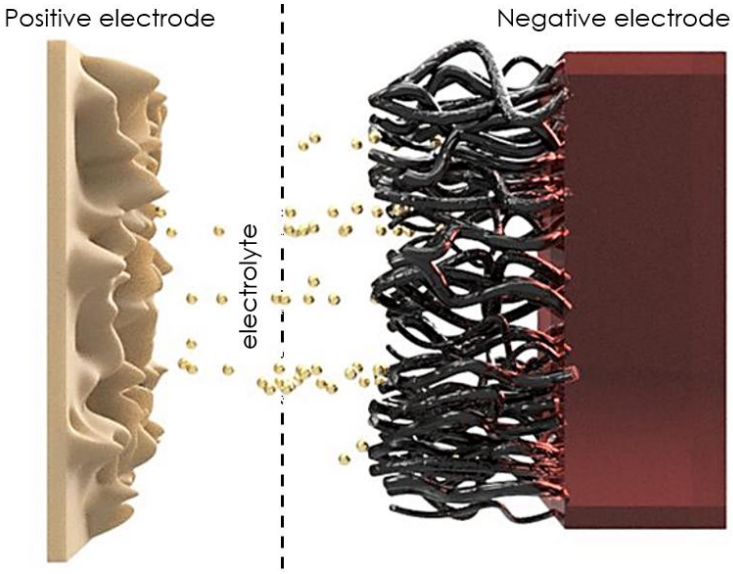

Figure 6: Schematic representation of the electrode and electrolyte interface in a supercapacitor device.

The storage abilities of supercapacitor devices are mainly governed by their capacitive performance and by operating potential window. The potential window normally depends on the type of electrolyte (aqueous, organic, room temperature ionic liquids or solid state

electrolytes), whereas the capacitance behaviour of the device is an intrinsic property of electrode active material. Transition MOx based electrode materials have been commonly exploited in SCs due to their active properties in high specific capacitance, excellent reversibility, and high energy densities[24]. In addition, their abundance and enhanced operating potential window makes MOx a future prospect in commercial outlook which needs further research and investigations.

It turns out that a hybrid energy storage device as a combination between double layer electrodes and pseudocapacitive electrodes can deliver high energy and power density compared to each type of SCs alone (asymmetric SCs). Overall, supercapacitors present the prospect of future energy storage systems with fast charge and discharge abilities, however it is genuinely required to increase their energy density for future applications.

CHAPTER 4

Metal oxide Thin-film Photovoltaics

One of the recently emerged modules in the field of PVs is based on thin-film architectures of ubiquitous MOx semiconductors. The remarkable optoelectronic properties and the versatility of fabrication methods by simple, low-cost and scalable processes confers MOx a pivotable role in next generation PVs. Moreover, the high **chemical stability** and **durability** of MOx can provide the requirement for a marketable PV device. So far, a wide range of known n-type or p-type MOx semiconductors (either intrinsically or doped) have been employed in fabricating all-oxide photovoltaics[25–28]. The favorable band gap of MOx permits utilizing the different spectral region of solar light ranging from UV, by employing wide-band gap semiconductors like ZnO (3.2 eV)[29], TiO_2 (3.2 eV)[28] and SnO_2 (3.8 eV)[30], to visible range and near infrared region (p-type light absorbers like CuO (1.4 eV)[29], Cu_2O (2.1eV)[30] and Co_3O_4 (0.7, 1.5, 2.1 & 4.4 eV)[31] semiconductors). The photoconversion mechanism in all-oxide PV modules (heterojunction or homojunction), is conventionally based on traditional p-n junctions in which the potentially built-up electron-hole pairs at the junction interface are collected by different contact electrodes.

Later to their compelling advantages in stability and low cost, all-MOx PV modules exhibit rather low conversion efficacies. So far, the highest PCE recorded in these devices is 6% and based on heterojunction of n-type aluminium–gallium–oxide and sodium doped Cu_2O[26]. One of the primary shortcomings in the MOx PVs, is the lack of p-type absorbers combining two characteristic of (i) suitable band gap, in accordance with ideal emission in 1.34 eV, and (ii) good carrier mobilities. For example cupric oxide (CuO), an intrinsically p-type MOx, is one of the promising candidates for photovoltaic absorber layer application. High optical absorption and the band gap of ~1.4 eV can attain to predicted theoretical efficiency of ~31%[32]. However, the low carrier mobility and high series resistance limits the PCE of fabricated PVs using CuO layer to ~1%[29]. Co_3O_4 (E_g=1.5

eV) is another interesting candidate for efficient absorber layer, although the merits of its application in MOx PVs, did not result in high PCE values[28].

One of the partial aims of this thesis work is to resolve some of the major shortcomings of all-oxide PVs using nanostructuring and interface engineering of the designed cells. The two following strategies includes (i) increasing the *carrier mobility versus incident light penetration depth* of p-type light absorbers by using single crystalline epitaxial 1D nanorods (NRs) forest. Parallel to this aim it is required to adjust the thickness of the p-type absorber to find the optimal points necessary for both adequate light absorption and sufficient carrier generations. This is also an important fact in the thin-film heterojunctions which pose *lattice mis-matching* in the junction with two dissimilar (as in crystal structure) semiconductors. The second strategy aims at increasing the photoexcited carrier generation in the device, exploiting the effect of (ii) *internal light trapping*. The scientific efforts which are explained in this section resulted in publication of the work ***"Vertically aligned Co_3O_4 nanorods as a platform for inverted all-oxide heterojunctions"*** (appendix I). The context of this chapter tends to describe a summary of the results and the underlying proof of concepts which exploited for tackling the efficiency hurdles in all-oxide PVs.

4.1. Light absorption and carrier diffusion tradeoff

The limited photo-excited charge collection in depth of the MOx semiconductor significantly reduces the possibility of exploiting thicker semiconductor layers. This phenomena is particularly evident/present in p-type light absorber MOx due to their intrinsic low mobility of minority carriers. In other words, the high electronegativity of the O atoms in the p-type MOx, causes highly localized O 2p orbitals as in their electronic structure, which prohibits the formation of the shallow acceptors[33].

Consequently, the designed heterojunctions based on p-type light absorbers, normally encounter severe light loss. Similarly, a rational solution is followed to designate the maximum photoconversion efficiency (PCE) of the planar all-oxide heterojunction devices by altering the thickness of the absorber material and determining the threshold between optimized light absorption and PCE values. A similar approached has been employed in our fabricated PV device based on Co_3O_4 NRs absorber layer[34]. One of the main parameters of investigation was to alter the thickness of Co_3O_4 NRs absorber layer to find

the optimal PCE values. Figure 7 (C) and (D) present a cross-section overview of the two fabricated heterojunctions based on Co_3O_4 NRs and TiO_2 n-type overlayer. The obtained photovoltaic parameters of the fabricated Co_3O_4 NRs/TiO_2 heterojunctions can be observed in Figure 7 (b). Our result indicated the highest open circuit voltage (V_{oc}) and short circuit current (J_{sc}) for the junction with 30 nm nominal length of the Co_3O_4 NRs Figure 8 (c) (thickness of the layers were experimentally determined using Rutherford backscattering technique explained in *Materials and methods* section). It is noted that, in all the fabricated nanostructures heterojunctions, the J_{sc} increases with the decrease of the Co_3O_4 NRs length. This fact can be attributed to the limited carrier mobility in the depth of Co_3O_4 layer, which induces charge recombination by increasing the length traveled by the holes inside the NRs absorber.

4.2. Lattice mis-matching in heterojunctions

The dictated need for variation of the thickness in heterojunctions is in its essence related to interfacing two semiconductor with dissimilar crystal structure. Conventionally, underlying physics of the p-n junctions anticipated interfacing two semiconductors which pose similar lattice constants. This was considered an essential requirement for defining the atomic level impurities in each n and p semiconductors. Since severe lattice miss-matching would cause interfacial dislocations and electronic defects such as interface traps. However, it was appeared that a good quality of heterojunctions, with dissimilar semiconductors, could still be achieved guaranteed that the employed layers are relatively thin[35]. This fact is schematically illustrated in Figure 7 (a) using imaginary cubic crystals with different lattice constants. In general, for a relaxed heterojunction with dissimilar semiconductors the lattice dislocations at the interface is a major drawback. However, if the layer is thin enough (generally grown by epitaxial methods which result in rather clean interface), the first few layers lattice constants are strained to the semiconductor substrate beneath and normally presents similar features. In that sense, normally the dislocations are eliminated and it is even possible to exploit wider range of semiconductors which naturally do not have similar lattice constants[36,37].

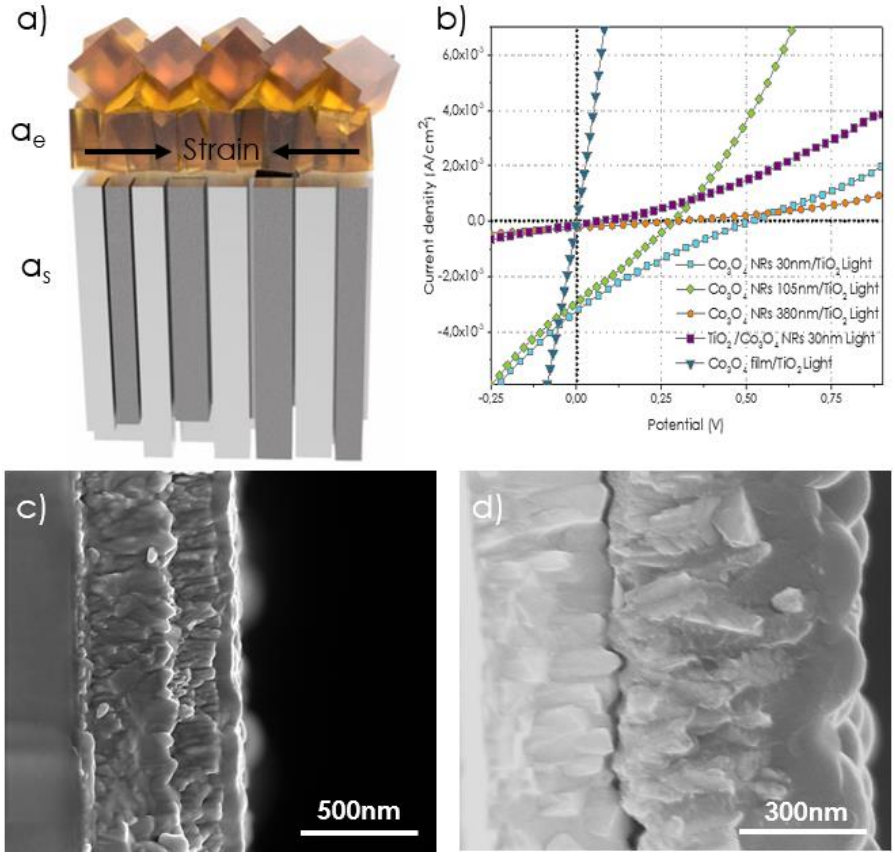

Figure 7: (a) Two materials with mis-matched lattice constant a_e and a_s. If the layer grown on material "s" is thin enough, the lattice constant of the "e" layer normally is strained to interface of the substrate material.

4.3. Light trapping

Another solution for the detrimental decrease of the light-loss while prevailing an efficient rate of photoexcited carrier generation is to use nanostructured platforms. 1D geometries such as nanowires and nanorods (NRs) are a useful alternative for employing efficient charge transport and at the same time enhanced decoupling processes for light absorption[38]. In addition, NRs geometry can remarkably increase the active depletion region for carrier generation in a relatively smaller area compared to thin film planar geometries[39,40]. Similarly, in the corresponding project work (*Appendix I*), we have exploited vertically aligned forest of Co_3O_4 as a 1D platform of p-type light absorber

(Figure 9, 8). The plasma assisted vapor-solid deposition technique of the Co_3O_4 NR arrays promoted the possibility of easily modulating the thickness of the p-type layer via altering the deposition durations. In our work three nominal thicknesses of the Co_3O_4 NR arrays of 30,105 and 380 nm were employed for PV analysing the subsequent fabricated heterojunctions. Conformally deposited TiO_2 (~290 nm thickness) is also exploited as the overlaid n-type layer. We have later compared the optoelectronic performance of this structure with a planar thin-film counterpart. The single crystalline structure provided a clean platform, which is rather crucial for the reduced interfacial recombination in efficient performing PVs.

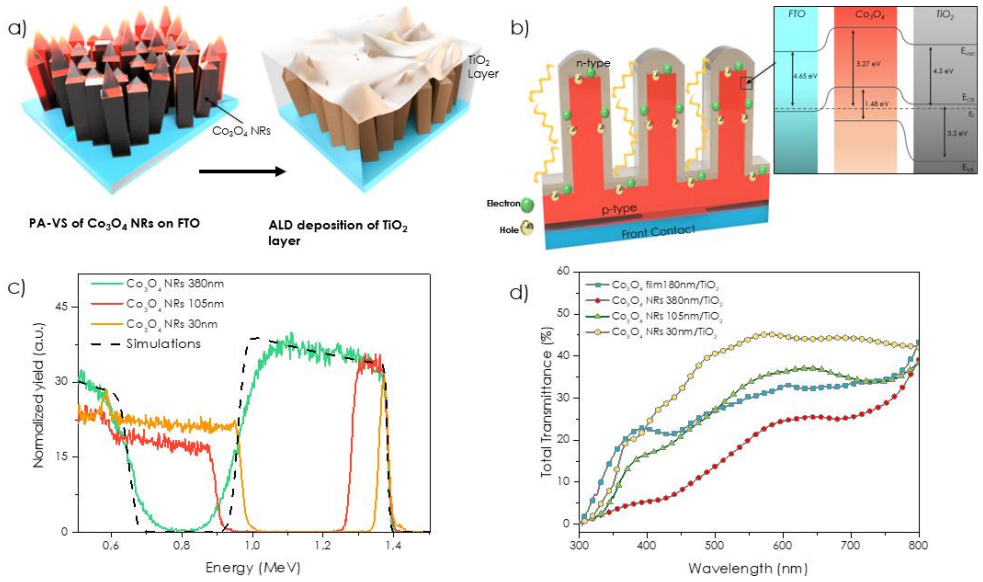

Figure 8: (a) Schematic illustration of the Co_3O_4/TiO_2 heterojunction architecture consisting of Co_3O_4 NRs platform and the overlaid TiO_2 layer. (b) The nanostructure morphology of the samples results in enhanced internal light trapping. (c) RBS spectra of the Co_3O_4 films deposited on silicon substrates. Total transmittance spectra of the Co_3O_4/TiO_2 NRs heterojunction compared with a planar thin-film heterojunction.

In addition, we have provided direct evidence that the vertically aligned configuration of 1D nanostructures in our heterojunction can create multiple internal scattering/reflection of the incoming light and increase the probability of light absorption and charge collection in significantly enlarged active depletion region of heterojunctions[41,42] as schematically

shown in Figure 8 (b). Our total transmittance results indicated that the 1D geometries of the Co_3O_4 provided higher light absorption even with lower nominal thickness compared to the polycrystalline thin-film counterparts, mainly thanks to increased light scattering induced by the 1D geometry (Figure 8 (d)). In this case our 380 nm Co_3O_4 NRs/TiO_2 heterojunction presents nearly 82% light absorption in the mid-visible range.

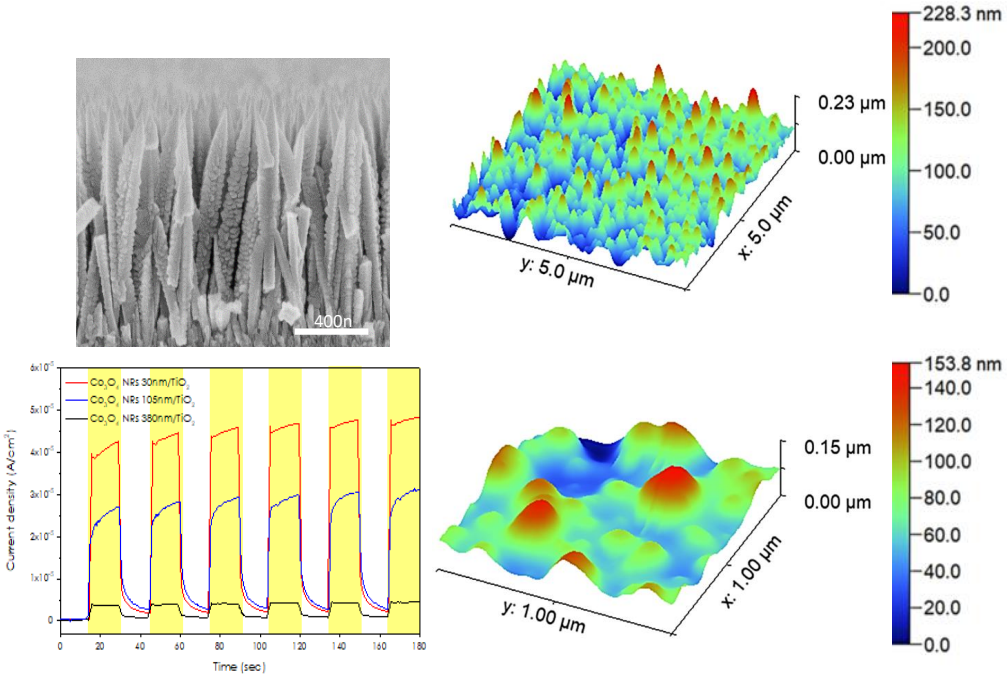

Figure 9: Showcasing the vapor-solid deposited 1D structures of Co_3O_4 NRs employed as p-type absorber semiconductor. The surface topology of the samples is characterized using atomic force microscopy and presented a rough and wavy nature of the heterojunctions with average roughness of 25±3 nm.

This feature can promote the possibility of using thin absorber layers, which impairs higher light absorption. In as similar fashion, the obtained AFM results demonstrates the rough morphology of heterojunctions with nanoscale surface roughness of ~25 nm with premises of high internal light diffusion. In agreement with the obtained *J-V* results, we have later demonstrated the effect of the Co_3O_4 NRs length on the carrier generation of the heterojunction samples. The photocurrent responses of the samples denoted the faster rise-time of the Co_3O_4 30nm/TiO_2 (1.06 sec) as opposed to the NRs junction with 380 nm

thick Co_3O_4 (1.6 sec), which demonstrated the faster carrier transport in shorter Co_3O_4 NRs. Our results significantly highlighted limited carrier mobility in the depth of Co_3O_4 layer, which induces charge recombination by increasing the length travelled by the holes inside the NRs absorber.

CHAPTER 5

Plasmonic Light Harvesting

In this chapter we introduce the photophysics and the figures of merit offered by plasmonic light-matter interactions, with emphasis in solid-state optoelectronic devices where plasmonic structures have been employed to augment the spectral absorption in semiconducting materials.

The study of the generically designed active plasmonic devices, requires a deep insight into interaction of light with free-electrons, typically in metals or highly-doped semiconductors. Plasmonic interactions are normally classified corresponding to the nature of their resonant behavior. Surface plasmons dephasing is generally attributed to the coherent electron oscillations, which are normally taking place in noble metal nanostructures, if an additional optical momentum is provided to their vicinity (i.e. due to external excitation on their plasmonic absorption profile). These oscillations are typically bound to the noble metal interface and delocalized along its surface[43][44][45].

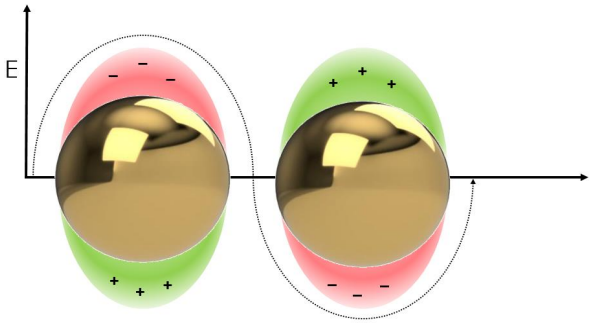

Figure 10: Localized surface plasmon resonance dephasing in a metal nanoparticle due to applied electromagnetic force generating electron cloud and positive cores.

5.1. Plasmonic devices

The optoelectronic properties of plasmonics has provided a great number of advances in a panorama of the fields, in the overview of light-matter interactions such as biology[46,47], photocatalytic chemistry[48][49], quantum processing[49] and energy harvesting[44,50].

Conventionally, the optoelectronic devices aim at three frameworks for employing plasmonic architectures. (i) Hot carrier energy conversion, through exploiting the non-thermal equilibrium electrons from surface plasmon dephasing of metal NPs. (ii) increasing the hot-electron injection yield of semiconductors which corresponds to the higher derived current in devices, i.e. conversion systems, and finally (iii) increasing the spectral absorption range of the optoelectronics by tunable light absorption of the plasmonic NPs. Overall, in all the allocated plasmonic devices the main challenge involves harvesting highly energetic electrons photogenerated in the metals, before their fast thermalized recombination, an effect that poses intrinsic limitation for large-scale applications of plasmonic waveguides[51,52].

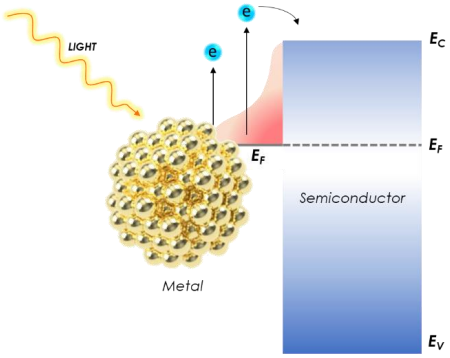

Figure 11: The hot-electron injection mechanism in a plasmonic metal/semiconductor junction.

To harvest the hot-electron population, one must collect the excited electrons before thermalization, meaning that the photogenerated carriers, need to reach the metal interface in a fast time-scale and retain high enough kinetic energy so they can be extracted. The hot-electron transfer phenomenon from metal to semiconductor is schematically shown in Figure 9.

Some of the early investigations of plasmonic hot-electron injection were reported in the fields of photocatalysis to extend the visible light spectral responses of TiO_2 due to its wide band gap of 3.2 eV. Within this approach, illuminated metal NPs that were adsorbed onto the TiO_2, inject hot-electrons in the anode and get replenished by a liquid electrolyte[53,54]. The early application of the plasmonic light harvesting systems in PVs where firstly reported in dye-sensitized solar cells employing gold and silver NPs on ZnO and TiO_2 electrodes[55,56]. It was only till Reineck et al reported the first investigations on solid-state plasmonic solar cells, where a hole-transport organic layer of Spiro-OMeTAD was used to collect the positive ionic hot-carriers subsequent to injection of the hot-electrons in TiO_2 semiconductor layer[57].

5.2. Hot-carrier harvesting architecture

One of the simplest architectures to harvest plasmonic hot electrons is the metal-semiconductor (MS) Schottky junction (Figure 11). In this approach, energetic electrons can be collected from the metal electrode provided they arrive to the interface with enough kinetic energy to overcome the existing barrier (Φ_{SBH}). The built-in field that exists in the semiconductor aids the injected electron to recirculate and recombine with a hole in the counter electrode thus generating a plasmonic-induced photocurrent. Due to its conceptual simplicity, several works made use of this structure to report hot-carrier collecting devices with reported implications as PVs or photodetectors[44,50].

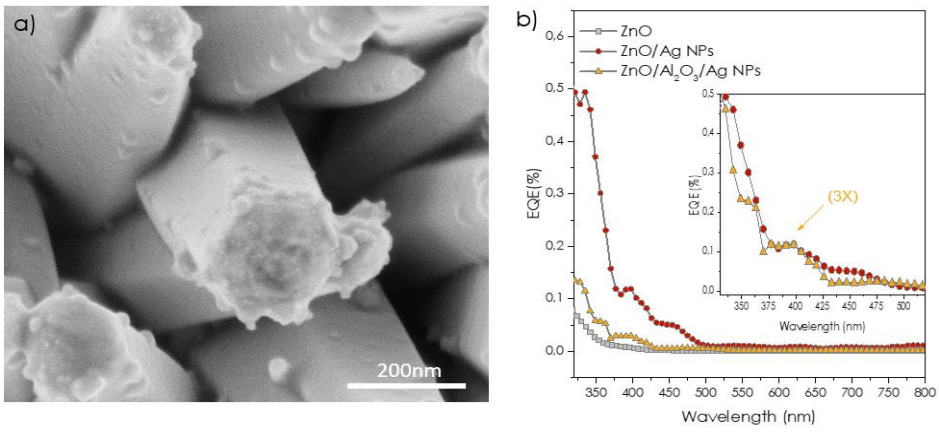

Figure 12: (a) SEM image of the grown ZnO NRs decorated with the silver NPs. (b) The external quantum efficiency (EQE) of the Ag decorated samples correlates well with the

plasmonic absorption profile of the silver nanoparticles and demonstrates the hot-carrier injection from silver NPs to ZnO NRs.

5.2.1. **Device architecture:**

In this research work we have employed a light harvesting 1D structure of the ZnO semiconductors and plasmonic silver (Ag) NPs, where we explore a deep insight into the hot-carrier collection mechanisms mediated by light. The attributed research article corresponding to this chapter, is appended further in this thesis (*Appendix II*) as ***"Optical Field Coupling in ZnO Nanorods Decorated with Silver Plasmonic Nanoparticles"***. The 1D architecture of the samples were considered so that, it can provoke an extended absorption of visible light through internal light trapping whilst promoting the fast collection of the photogenerated plasmonic hot-carriers of Ag NPs as a result of fast intrinsic carrier transfer abilities of the epitaxial NRs structure. An overview of the prepared samples morphology is shown in Figure 12 (a). Our results indicated that, the hydrothermally grown ZnO NRs decorated with electrodeposited plasmonic Ag NPs, resemble a simple and yet superior plasmonic Schottky metal/semiconductor properties with prospects of higher carrier collections.

5.2.2. **Photocurrent generation:**

Hot-carriers are generated in the Ag NPs, corresponding to their geometry and interface assembly of Ag NPs on ZnO NRs, a fraction of separated electron-hole pairs are injected to the ZnO substrate until they reach the FTO glass for collection. The derived external quantum efficiency (EQE) measurements of the Ag decorated samples (Figure 12 (b)) presented features corresponding to plasmonic absorption of the Ag NPs which translated in to photogenerated current in the composite samples. Our result shows that the ZnO NRs platform serves as an efficient substrate that yields a hot electron photocurrent of about 75% compared to bare ZnO, with a maximum EQE of 0.5% at the plasmonic absorption of Ag NPs. This showcases the feasibility of our composite system for active plasmonic sensing, yet still not sufficient for energy conversion.

In this section we have successfully demonstrated that the ZnO NRs/Ag NPs junction can be an interesting device for hot-carrier photodetection. On the other hand, an energy conversion device requires a simultaneous supply of current and voltage. Yet we identify the metal/semiconductor interfacial design in this system requires a correct architecture

suitable for collecting the seperated positive and negative charges (circuit permission), to originate V_{oc} values. This fact will be discussed further in the next sections.

5.3. The plasmonic induced hot-carrier injection

Previously in this chapter we have discussed the mechanisms of the hot-carrier generations in plasmonic NPs. The term hot-carrier in plasmonics indicates the electrons that are not in thermodynamic equilibrium. As mentioned before, these hot-carriers can generate photocurrents in an optimally designed system of semiconductor and plasmonic NPs. Here, in this section we discuss the main carrier transfer mechanism inherent to the plasmonic NPs and we provide direct evidence of the obtained transfer data in the present research.

Preliminary, the dephasing transfer in plasmonics are categorized into two competitive ways of *radiative emissions* and *non-radiative* relaxations. The non-radiative relaxation, normally quenches in the environmental medium through electron-electron, electron-phonon, electron interface interaction or scattering[58,59]. The hot-carriers which are generated through non-radiative relaxation processes, can result in intra- and/or interband excitation in the vicinity of an adjacent semiconductor and be transferred to its conduction band. Of course, it should be noted that the intra- or interband transitions requires an energy band overlap between the particles localized surface plasmon resonance (LSPR), and the semiconductor. The non-radiative charge injection from plasmonic NPs towards semiconductor is normally described by two competitive mechanisms as (i) direct electron transfer and (ii) plasma induced resonance energy transfer (PIRET) processes. Below we describe each of these two processes individually with indications into our own research project, and showcasing our sample design in order to comprehensively distinguish these two phenomena.

5.3.1. **Direct electron transfer (DET):**

The energies of the hot-carriers have a wide distribution range corresponding to the type of the noble metals and their nanoscale morphology. Typically, the approximate LSPR energy of the Au or Ag, two of the most common plasmonic materials are ranged between 1eV to 4eV. In a normal Schottky junction such energetic carriers can overcome the barrier height (Φ_{SBH}) and may migrate to the semiconductor CB, a transfer which is opposite to

the defined transfer direction in a Schottky system (from semiconductor conduction band towards Fermi level of the metal). A preview of this transfer process is illustrated in Figure 13 (a).

5.3.2. **Plasmonic induced resonance energy transfer (PIRET):**

Second picture in plasmonic non-radiative carrier transfer is derived from Fermi's golden rule in electric dipole approximations[60,61].

$$\Gamma_k^0 = \left(\frac{2\pi e^2}{h}\right) E_0^2 |p_{mk}|^2 \, \delta(E_m - E_k - hw) \tag{5}$$

Where Γ_k is the total transition rate of the vector k, E_o corresponds to the intensity of the electric field of incident light and p_{mk} is defined as momentum matrix element. The E_m and E_k components represent the initial and the final energy states of the electron transitions.

In that perspective, the large dipole moments formed in plasmonic NPs, due to photoexcitations, can induce the dipole moments in the neighboring semiconductors. Clearly, this form of carrier transfer, does not necessarily require the direct contact between the metal NPs and the semiconductor, yet a detrimental distance for dipole moment transfer is essential. Here we refer to detrimental distance as the optimized distance between plasmonic NPs and the semiconductor, which permits a satisfactory dipole-dipole interactions.

In our dedicated research, we have exploited a simple design solution, in order to systematically investigate the PIRET mechanism. The solution involved preparing two sets of samples of which (i) plasmonic Ag NPs are in direct contact with a semiconductor and (ii) second set of sample with a passivating 4 nm Al_2O_3 layer in between ZnO and the Ag NPs. Study of the photoexcited carrier transfer in the former system with conformal deposition of Al_2O_3 intermediate layer, permits a distinct separation of PIRET carrier transfer mechanism from DET processes. To further understand the mechanism of photoinduced carrier transfer in details, characterization methods such as transient absorption spectroscopy in the femtosecond and picosecond time regimes are of great use.

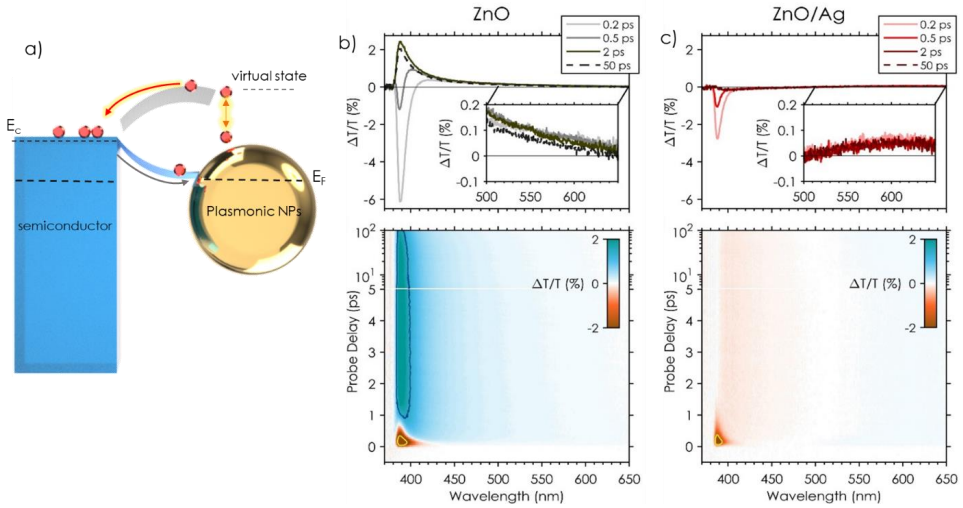

Figure 13: (a) Schematic view of the possible transfer routes in a plasmonic Schottky system (The grey arrow corresponds to the Schottky carrier transfer phenomena from Ag NPs to semiconductor). (b),(c) Differential transmission spectra of the ZnO NRs and the Ag decorated samples in different time intervals. The samples are pumped with the 266 nm laser corresponding to the interband absorption edge of Ag NPs.

Due to very fast transitions of the photoinduced carrier transfer in the Schottky plasmonic systems (picoseconds or hundreds of femto seconds), we have studied the details of the carrier redistribution mechanisms in our samples using transient pump-probe spectroscopy (Figure 13 (b), (c)). The samples were excited with the 266 nm laser which tend to target the plasmonic excitation of the Ag NPs via interband transitions. The differential transmittance (ΔT/T) spectra of the ZnO NRs presented a sharp photoinduced absorption (PA) at around 380 nm corresponding to band filling of the ZnO near band-edge states. The recorded spectra rapidly evolves to the positive direction in a decay form after 1 ps reviving a photobleaching (PB) signal in the TT spectra. We assign this behavior to the band filling of the ZnO NRs band edge (BE) filling. Thus in longer probing times, more than 1 ps, we recognize the TT behaviour of the bare ZnO NRs with two PB signatures of (i) between 389-420 nm and a (ii) broad tail centred at 610 nm corresponding to BE filling and the defect state emissions of the ZnO NRs respectively. We have observed a similar trend for the Ag decorated sample in the first 300 fs a negative PA emission centred at 389 nm corresponding to BE of ZnO and a second broad PB ascribed to defect states centred at 620 nm (Figure 13 (C)). On the other hand, in the longer life-times 2 ps

the TT evolution of the ZnO/Ag BE differs significantly from that of bare ZnO. Our recorded spectra indicated that the PA emission of the ZnO/Ag NPs at 389 nm, will never evolve to the positive PB signal, similar to what was observed in bare ZnO NRs, even after 50 ps of the probing delay time. In our result, we indicated this behaviour of the ZnO NRs/ Ag sample to the band gap renormalization (BGR) processes due to plasmonic excitation of the Ag NPs. BGR in a transient form in normally manifested due to modification of the electronic band structure and the excitonic binding energy of the materials (in our case ZnO), as a result of the populated carrier injection of the Ag NPs. We determined that the time-scale of BGR in our TT spectra is rather cohesive with the plasmonic time-scale of the Ag NPs. In that sense, we have further highlighted the TT evolution of the samples in the critical time-scales between PA and PB transitions (Figure 14 (a)).

5.4. Carrier transfer mechanisms and injection yield

This section describes recent research progress into plasmonic hot-carrier current yield of the synergic system. In general, one of the main challenges in plasmonic hot-carrier devices, such as photodetectors or PVs is to convert the photogenerated carriers into deliverable current. This leads to the collection of very fast decoupled plasmonic carriers in the adjacent semiconductor and converting them into usable current. In another word, optimizing the trade-of between carrier generation and the carrier injection in the composite system. In that sense it is rather important to fully comprehend the carrier transfer mechanism in a hot-carrier system and to distinguish which transfer processes result in output non-radiative photocurrent generation in the device (it should be noted that the desired non-radiative photocurrent is rather suitable for the direction of our work (PVs, Photodetectors) and the other hot-carrier radiative transfer processes such as Förster resonance energy transfer might be applicable in different fields).

Figure 14 (a) and (b) demonstrates the transient dynamics of the ZnO NRs at the bottom of the initial ZnO negative BE emission at 389 nm and around the central region of the defect states (575 nm) corresponding to the maximum of the PB shoulder. Looking to the recorded spectra, contributions of the PB in the BE region of the ZnO and ZnO/Ag sample are vividly modified due to presence of the plasmonic Ag mainly in initial delay times below 300 fs. We have observed a very small PB in the delay times near 200 fs (Figure 14 (a)inset) for both samples. However, the Ag decorated sample presented an exponent

decay as opposed to the bare ZnO NRs indicating a longer carrier redistribution mechanism in accordance with the LSPR decay time of the Ag NPs (*Appendix II* transient spectra of bare Ag NPs). In addition, the PA dynamics of the Ag decorated ZnO sample at around 2 ps presents a smaller amplitude decay compared to bare ZnO which further approves our hypothesis on the BGR effect due to LSPR dephasing of Ag NPs increasing the excitonic density of ZnO conduction band. Moreover, the TT signal of the Ag decorated sample after PA band filling never reaches the positive sign (no significant PB is observable), which again verified the BGR effect as a result of fast electron recirculation favoured by the small energy difference between the conduction band of ZnO and the Fermi level of Ag.

5.4.1. **PIRET or DET?**

As mentioned before in order to distinguish the DET and PIRET processes we have exploited a ~4 nm Al_2O_3 intermediate layer in between ZnO NRs and Ag NPs. The recorded photoresponse of the composite samples under controlled illumination, via low pass optical filters, targeting the different region of the plasmonic absorption of the Ag NPs is presented in Figure 14 (c-d). It is evident that the alumina layer, responsible for surface passivation, is also modifying hot-carrier injection as can be observed by the amplitude of the obtained photocurrents. We previously verified the reduced EQE of Al_2O_3 integrated devices compared with the one obtained in the absence of Al_2O_3. The EQE of the Ag integrated sample without Al_2O_3 spacer layer, presented 75% higher deliverable photocurrent and 0.5 % EQE in the region of Ag NPs plasmonic absorption (Figure 12 (b)). We have assigned the increase in the EQE of the samples to the combination of the DET and the PIRET dipole-dipole hot-carrier transfer mechanism of Ag NPs to ZnO NRs.

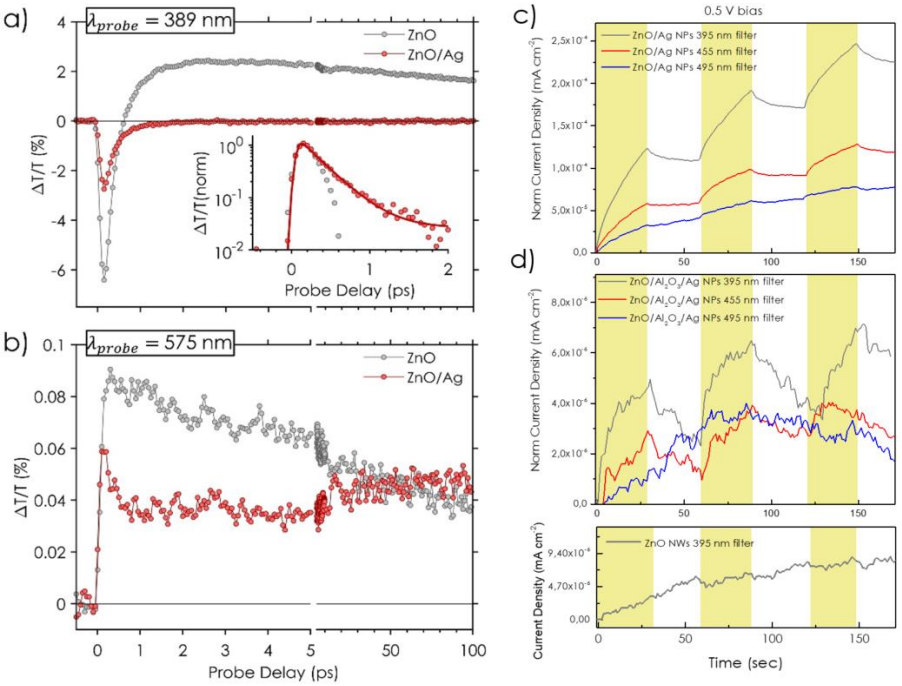

Figure 14: (a) Differential transmittance spectra of the bare ZnO NRs and the ZnO NRs/ Ag samples at probe wavelengths corresponding to band-edge emission of ZnO (389 nm) and the defect states (around 575 nm). (b) Light-responses of the samples with and without Al_2O_3 intermediate layer, under selective illumination using low pass filters, indicates the role of interfacial design on plasmonic carrier injection.

Our photoresponse results indicated a nearly 13% higher current yield in ZnO/Ag NPs compared with the bare sample. Notably, in both EQE results (Figure 12 (b)) and photoresponses of the Al_2O_3 integrated samples (Figure 14 (d)) we still observe a reasonable current response even without a direct contact between Ag NPs and ZnO NRs. In this case we have considered the hot-carrier transfer mechanism of Ag NPs apart from DET mechanism and solely to dipole-dipole transfer processes or Fowler-Nordheim tunneling of energetic electrons. Since both dipole-dipole PIRET transfer and Fowler-Nordheim tunneling, present the same energy profile and the temporal evolution, the subjects of their essence is still under intense debate in the community, and full quantitative descriptions of hot-electron injection are still not within reach.

CHAPTER 6

Graphene/metal oxide junction (a remedy?)

Research findings in this chapter, describes the photophysics and the optoelectronic properties of the graphene and semiconductor (specifically MOx semiconductors) junctions. Initially we explain the electronic properties of the constituent hybrid junctions and later we highlight the corresponding research direction in this thesis by showcasing the dedicated research carried out. The denoted research article corresponding to this chapter ***"In-depth Carrier Transport In Barrier Variable Iron-oxide And Vertically Aligned Reduced-Graphene oxide Composite"*** is further attached as *Appendix III*.

The contact between basal plane of graphene and the MOx semiconductors, enables the origin of a surface junction with intrinsic driving potential to transfer the charges across the bulk of consequent layer[62]. This phenomenon can clearly provide a guideline for improving the optoelectronic performance of the MOx based devices, specifically the photexcited carrier transport properties. As mentioned in the previous chapters, despite prominent advantages of all-oxide optoelectronics, fulfilling two important criteria of stability and low cost, the efficiency of the produced PV modules is rather low. In this framework, the main shortcoming compromising the efficiency of the fabricated MOx light harvesting systems, is believed to be associated with the limited mobility of minority carriers in absorber layers. We have exploited the vertically aligned flakes of graphene scaffold, a photo conductive 2D material, as platform for reviving thereof. Below we briefly

discuss the theory and the properties of the hybrid-composite system and subsequently we move on to the associated results.

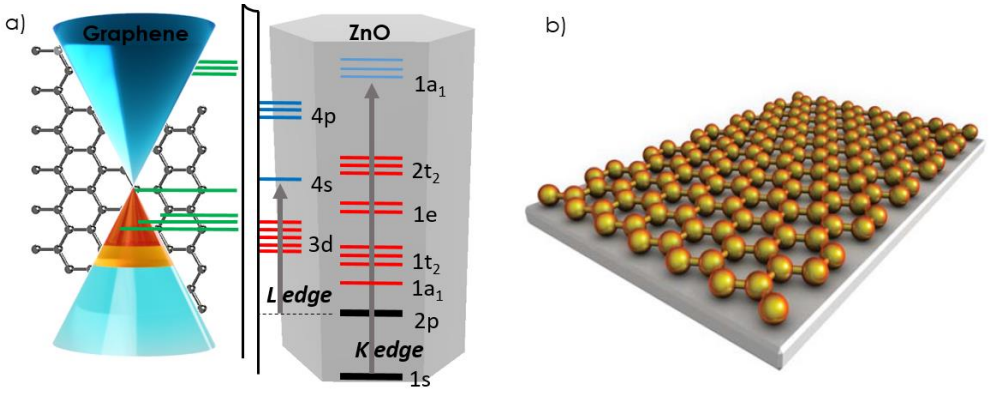

Figure 15: (a) The band diagram of the ZnO semiconductor in contact with pristine graphene. The carrier transfer from ZnO to graphene, creates a downward band-bending in graphene and alters the population density of the junction. (b) Graphene sheet interfaced with semiconductor creating an active surface.

Graphene, a single layer atomically thin allotrope of carbon has demonstrated an immense potential for next-generation high performance electronic and optoelectronic devices. The distinctive band structure and intrinsic driving potential to transfer carries has enabled different architectures of graphene/GDs such as single layer graphene, few layers stacked graphene and bilayers of GDs to be interfaced with various structures of semiconductors[63–65]. Typically few main pathways are ensued by implementing graphene in optoelectronic devices. Therefore, understanding the over-ruling mechanisms of graphene/semiconductor interactions in these pathways, can promote the performance of the future devices.

6.1. The role of graphene in energy-band engineering

One of the appealing properties of graphene/semiconductor junctions is the effect of carrier transport phenomena in interfacial band engineering of the devices. Interfacing graphene with semiconductors can give rise to unique properties which venues to an atomically thin light-responsive active surface below the graphene.

Conventionally, the junctions of graphene and bulk semiconductors were considered as typical metal/semiconductor Schottky junction of which the high position of Fermi level

in metals caused the over potential for directional charge extraction. Moreover, due to high density of states, the Fermi level height of metals remain unchanged through charge transfer phenomenon (Figure 16 (a)).

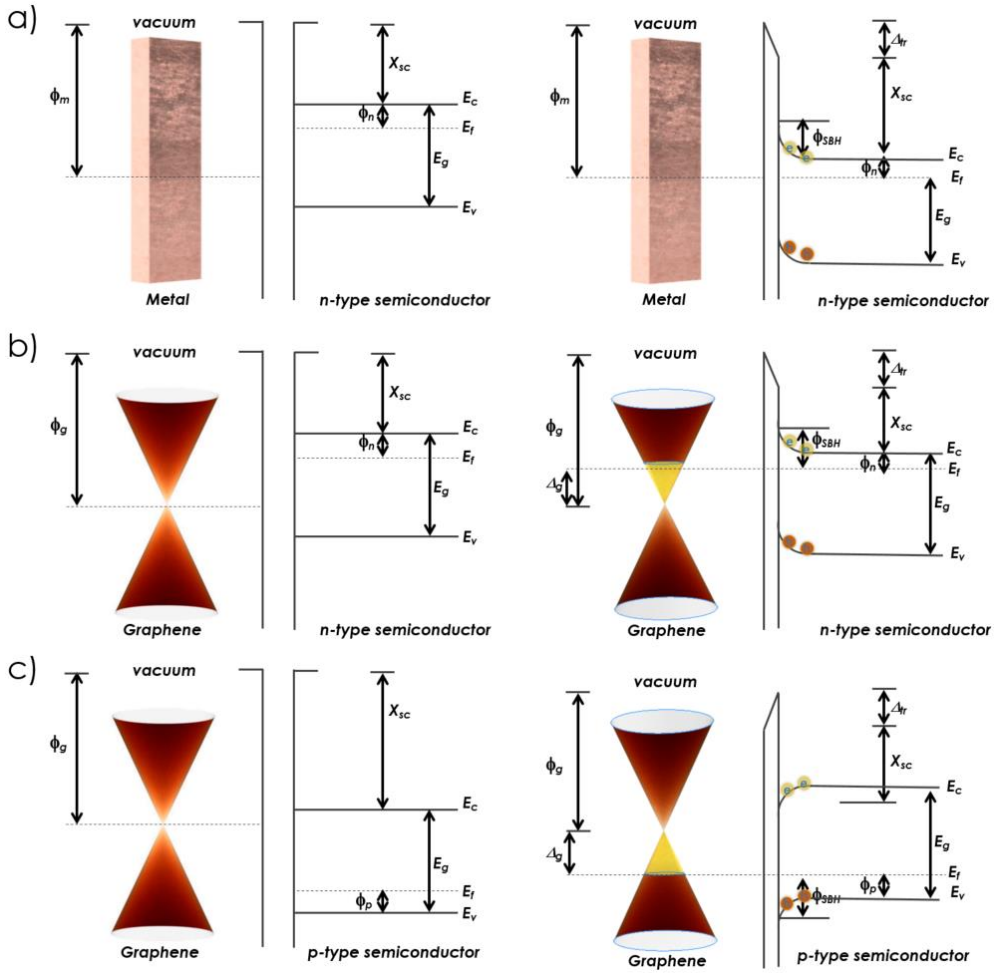

Figure 16 : Band energy diagram of the n-type and p-type semiconductors interfaced with (a) metal and (b,c) graphene.

However, carrier transport in graphene/semiconductor junction is rather different compared to traditional Schottky junctions. Defect free single layer graphene can present a Fermi level and maximum density of states that are exactly leveled with Dirac points (so called zero band gap semiconductor). The transfer of charges from semiconductor to

graphene will result in shift of Fermi level in graphene and reduction of Schottky barrier heights (ϕ_{SBH}) for both adjacent n-type and p-type semiconductors. Correspondingly, graphene energy level will shift contradictory to the direction of charge transfer (for instance graphene behaves as a hole-doped semiconductor in a junction with n-type silicon) resulting in formation of a rectifying Schottky junction[62,66]. Essentially graphene/semiconductor junction can be beneficial for directional charge extraction, reducing the Schottky barrier heights, and increasing the electron-hole separation by increasing active depletion surface.

In general, the Schottky barrier height in graphene/semiconductor junction can be calculated experimentally (using Schottky diode relations) by determining the voltage (V)-current (I) characteristic of the junction:

$$I = AA^*T^2 \exp\left(-\frac{q\phi_{SBH}}{KT}\right)\left[exp\left(\frac{qV}{\eta kT}\right) - 1\right] \quad (6)$$

Where A, A^*, T, q, k, and η are the Schottky contact area, the Richardson constant at room temperature (300 K), electron charge, Boltzmann constant, and the ideality factor, respectively.

A more relativistic approach can also be asserted by considering the thermal equilibrium in the depletion region[67]. In that sense, graphene is treated as hole-doped due to charge transfer from n-type semiconductor. Hence, transferred charges (q_g), necessary for Fermi level shift (Δ_g) in graphene can be obtained by;

$$q_g = -q.sign(\Delta_g)\int_0^{q\Delta_q} \rho(E)dE = -\frac{1}{2}sign(\Delta_g).q^3 D_0\, \Delta_g^2 \quad (7)$$

In which D_o is the density of the state in graphene before Fermi energy level shift. q and Δ_g represent charge of the electrons and work function shift of graphene corresponding to charge transfer. Furthermore, the space charge (q_s) in the depletion layer is determined by:

$$q_s = sign\left(\phi_{SBH} - \phi_n - \frac{kT}{q}\right)\sqrt{2nq\varepsilon_r\varepsilon_0\left|\phi_{SBH} - \phi_n - \frac{kT}{q}\right|} \quad (8)$$

ϕ_n represents the energy difference between conduction band of semiconductor and its Fermi level as depicted in Figure 16. Where, ε_r and ε_o are the dielectric constant of

semiconductor and graphene, respectively. Considering the ideal state of materials, with no surface states and recombination, the total charge is equal to zero. The corresponding relation can determine the ϕ_{SBH} of the junction as a function of charge transfer.

$$q_g + q_s = 0 \tag{9}$$

6.2. The origin of photoconductivity in graphene

The origin of the photoresponse in graphene junctions has been studied extensively and is attributed to either thermoelectric or photovoltaic effects. Thus far, two relaxation mechanisms of electron-phonon and electron-electron scattering are assigned as the main cooling channels for photoexcited graphene[68–70]. On the other hand, electron–electron scattering, is denoted as the dominant mechanism of photocarrier energy relaxation, where the photoexcited carriers multiply while decaying towards an elevated electronic temperature. Up to now, several optoelectronic devices have been fabricated exploiting unique features of graphene such as zero energy gap, efficient transport and optical properties[71–73]. One appealing direction in use of graphene derivatives lies in light harvesting devices such as photonics and optoelectronics, where the combination of its unique optical and electronic properties can be fully exploited. Up to now, the GD have been employed in several PV devices including; (i) transparent conducting film[74], (ii) active light harvesting material for heterojunction[75], (iii) counter cathode electrode for dye sensitized PVs[76] and (iv) hole-transporting material for hybrid perovskite PVs[77]. However the main purpose of exploiting GD in the aforementioned devices, are normally corresponding to either energy band engineering of the adjacent semiconductors and/or conductive illumination platform, which normally re quires GD in planar architecture.

Despite the literature focus on the planar junction, in our dedicated work we have intended to employ the photoexcited carrier-carrier scattering relaxation mechanism of graphene, in order to promote the carrier transport in a less optically active MOx semiconductor light absorber. In that sense, we have fabricated a crisscross network of reduced graphene oxide (rGO), vertically aligned toward the illumination direction, and embedded in the thin-film structure of Fe_3O_4 semiconductor. A schematic illustration of the samples structure is presented in Figure 17. The amount of the crisscross in rGO scaffold underneath the Fe_3O_4 is rather detrimental to find the threshold for optimized mediated carrier transfer in photoexcited semiconductor. In that sense, we have arranged

to alter the amount of rGO by varying the number of cycles required for electrodeposition of the rGO network.

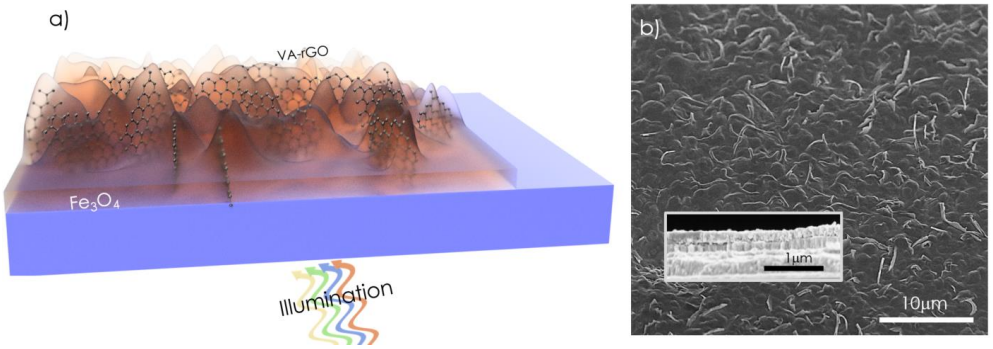

Figure 17: (a) Schematic view of the vertically aligned rGO scaffold embedded in the semiconductor film. (b) Planar view of the rGO integrated Fe_3O_4/Cu_2O heterojunction. (Inset) cross-section of the bare Fe_3O_4/Cu_2O sample identifying the nominal thickness of 100 nm for each layer.

6.3. Photoexcited carrier transfer

The efficiency of the light conversion process in graphene/semiconductor junctions is directly related to the fact that graphene structure dominates the carrier-carrier relaxation pathways as oppose to competing pathway dynamics of electron-phonon scattering and/or thermalization losses. In order to investigate whether the photoexcited carrier-carrier scattering process in graphene is actually contributing to the carrier transfer of the hybrid junction, we studied the current output of the system. We have provided the local current maps of the VA rGO/Fe_3O_4 surface, using intermodulation conductive force microscopy (ImCFM) where non-linear current-voltage maps of the samples can be collected with high spatial resolution over an extended area. The obtained results indicated a significant enhancement of the retrieved current in the areas attributed to the ripples and curls created by the rGO scaffold beneath as shown in Figure 18. Our measurements pointed out that the transfer of the charges in rGO scaffold, can mediate the carrier transport in-depth of the adjacent semiconductor interface as a result of carrier redistribution and/or carrier multiplication in rGO flakes. We noted the uneven current output of the samples on the areas with rGO scaffold and we have assigned this behavior to the (i) irregular geometries of the rGO network and (ii) the anomalous surface potential

effect as result of inhomogeneous carrier transport in-depth of the Fe_3O_4 semiconductor layer.

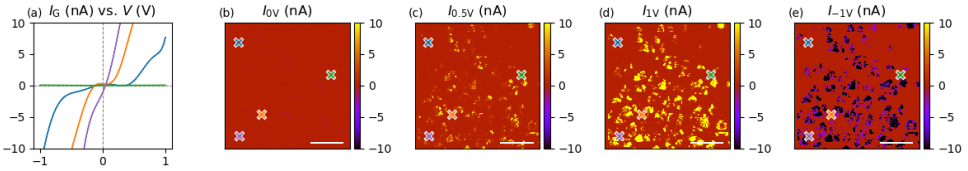

Figure 18: (a) The local J-V curves of the sample corresponding to the different region on the VA rGO/Fe_3O_4 surface (the considered points are marked on the right side maps). (b)-(e) The ImCFM current maps of the VA rGO/Fe_3O_4 in different forward and reverse bias. The brighter regions are corresponding to the VA rGO scaffold underneath the surface with significant increase in derived current.

6.4. Optical absorption in the graphene junctions

Electronic coupling of graphene atop of semiconductor can result in interfacial energy-band reorganization which can create a light-sensitive device. The high carrier-carrier scattering momentum in graphene can mediate energy transport which dominates the photoresponse in graphene integrated devices and manifests itself as increased quantum efficiencies. The surface photovoltage (SPV) spectra of the VA rGO integrated samples were compared with the bare semiconducting films in Figure 19.

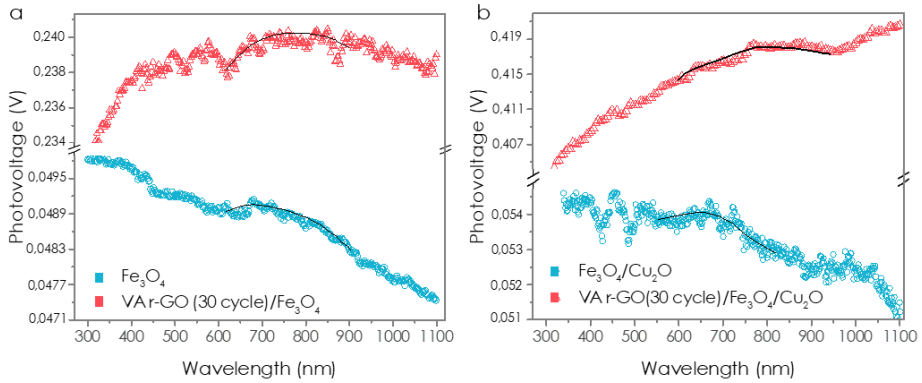

Figure 19: (a) SPV spectra of the VA rGO Fe_3O_4 of the sample presents drastically higher light-mediated potential in a wide range of excitation compared to bare Fe_3O_4. (b) The SPV results of the VA rGO integrated heterojunction as oppose to the bare

heterojunction. The black remarks in the SPV curves of the samples correspond to the energy-band transitions of the semiconductors (further explained in the text).

Our obtained data indicated a drastically higher photovoltage over a wide range of visible excitation which nearly extends over the entire visible region for VA rGO integrated sample. We have assigned the wide range of optoelectronic response in the samples to the increase in potential relaxation cascade beyond the optical band-gap of the VA rGO integrated Fe_3O_4 films to two possible mechanisms of (i) carrier-carrier scattering of graphene contributing to carrier generation/transport in Fe_3O_4 and (ii) charge trapping in the VA rGO network. Similar behavior is observed on the hybrid heterojunction sample, VA rGO (30 cycle)/Fe_3O_4/Cu_2O, where an enhanced SPV values are observed in the visible range. We have attributed the SPV increase in both VA rGO (30 cycle)/Fe_3O_4 and VA rGO (30 cycle)/Fe_3O_4/Cu_2O sample to the non-uniform photoexcited carrier transport in-depth of the films also known as anomalous surface photovoltaic effect. We exemplify that the intervention of the VA rGO network underneath the samples can cause the anomalous carrier transport in-depth of the system as a result of inhomogeneity in graphene sheets geometry and the non-uniform carrier redistribution in the bulk of the films.

CHAPTER 7

MOx for electrochemical energy storage

To achieve a sustainable society with an energy mix primarily based on solar energy, we need methods of storing energy from sunlight as chemical fuels. Photoelectrochemical storage devices offer the promise of energy proliferation which can be used to the extent of demand in any desired applications. Further in this section we present two research articles which provide the prospect of MOx materials as electrodes with significant Li ion storage ability which can provide pathways for a new concepts of direct solar storage. The research articles corresponding to this chapter, ***"Plasma assisted vapor solid deposition of Co_3O_4 tapered nanorods for energy applications"*** further attached as *Appendices (IV)* and ***"Direct solar conversion to energy storage; integrated solar supercapacitor"*** is an ongoing manuscript draft with attached results in this chapter. This section of the thesis focuses on two main determining roadmaps concerning the application of the MOx as capacitive electrodes for Li^+ ion storage systems. (i) We study the effect of design and different structural parameters on the storage ability of the electrodes and their optoelectronic behavior. (ii) Later we offer a design solution for a hybrid system for direct photo-carrier storage, by inspecting the origin of the MOx photo-spectral response and their dual functionality as light-absorbers and capacitive electrodes.

In both of the research articles, Co_3O_4 nanostructures have been a prominent focus due to it's versatile applications as high capacitance electrode materials with long cyclability[19] and more importantly as a suitable p-type light-absorber semiconductor[78,79] (previously exploited as p-type light absorber *appendix I*).

7.1. The effect of structural engineering in capacitive behavior

Unlike batteries and fuel cells that harvest energy stored in chemical bonds, supercapacitors exploit the electrostatic separation between electrolyte ions and high surface area electrodes. The amount of energy stored in supercapacitors is linearly proportional to the capacitance of the electrodes, which is rather interconnected to the specific surface area of the electrodes, making material optimization rather crucial.

$$C = {}^{\varepsilon A}/_{d} \tag{10}$$

Where A is the electrode surface area accessible to electrolyte ions, ε is the electrolyte dielectric constant and *d* is the diffusion separation length. Since surface area is explicitly important, understanding its effect on specific capacitance is rather crucial and has been a subject of study in our research.

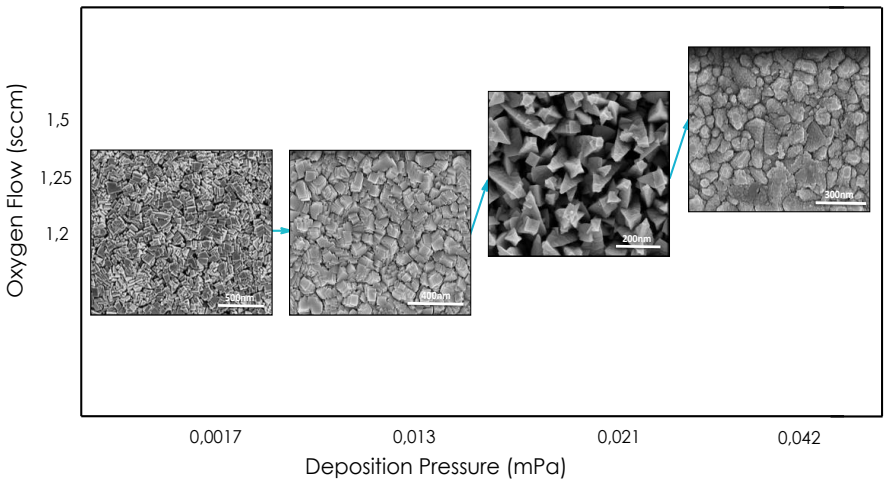

Figure 20: Different architectures synthesized via tuning the deposition pressure using PA-VS method.

In our work we have managed to synthesize different nanostructured architectures of Co_3O_4 electrodes using a newly developed method based on plasma assisted vapour solid (PA-VS) deposition technique. The PA-VS method implemented in our work provides a facile one-step solution to deposit various single-crystalline nanostructures of functional

materials with a higher deposition rate compared to several techniques. The morphological properties of some of the fabricated Co_3O_4 nanostructure electrodes, designed via simply tuning the deposition pressure are shown in Figure 20. We have selected the 1D NRs structures of the Co_3O_4 as the promising structure for their application as negative electrode for supercapacitors. The nominal length of the NRs structure, determining the active surface area for Li^+ adsorption and desorption process, were considered as the main subject of study. In that sense, we have investigated the trade-off between the length-dependent (thickness of the electrode) conductivity of the NRs and the increase of the capacitance due to enhanced porosity of the electrodes.

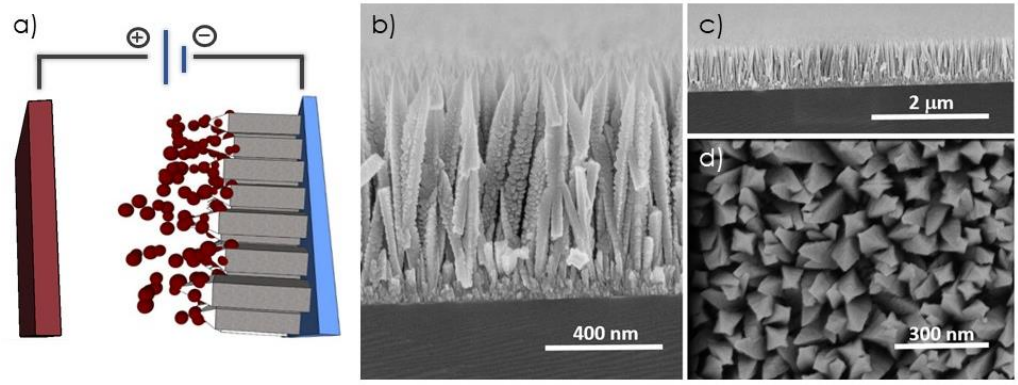

Figure 21: (a) Schematic illustration of the fabricated Co_3O_4 NRs performing as negative electrode as in electrochemical setup. (b)-(d) The morphological structure of the 700 nm Co_3O_4 NRs deposited on a Si substrate.

The obtained result indicated that the NRs with the highest thickness of the Co_3O_4 (Figure 21), corresponding to the highest surface area compared with the other nanostructured counterparts demonstrate the best Li^+ ion cyclability. The electrochemical characterization of the sample presented high stability of the electrode with no chemical or Faradic reactions noted on the sample in the considered potential window (Figure 22). The galvanostatic charge–discharge curves of the 700 nm Co_3O_4 NR electrode, as a prime candidate for the best electrode performance, under different current densities presented nonlinear pseudo-capacitance behavior with relatively high discharge rate. The features of the curves and the time cycles of the discharge and charge trends verified a high rate of Columbic reversibility in the electrodes, approving the limited current-voltage loss in the system. We have attributed the overall capacitance of the designated NR electrodes in this

work to the formation of solid electrolyte interface (SEI) layer, and as a result of diffusion of ions to the electrodes.

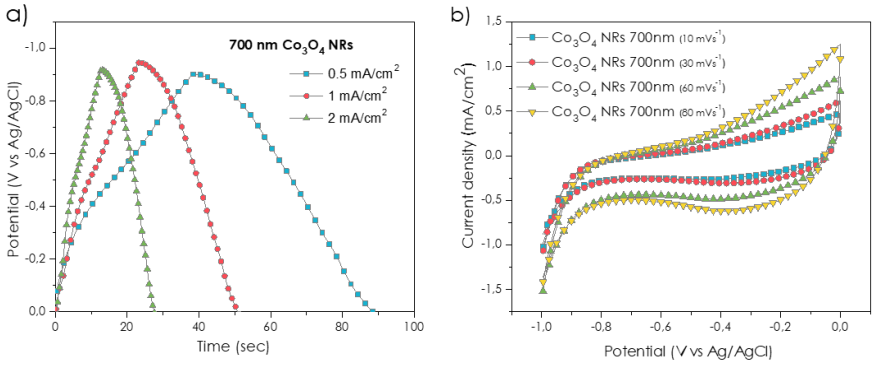

Figure 22: (a) Charge-discharge profile of the nanostructured samples. (b) Recorded cyclic voltammetry spectra of the fabricated NRs at different scanning rates indicated the high stability and the notable capacitance of the electrodes.

Electrochemical storage devices that can directly convert the solar radiation to the stored energy would offer a new approach for balancing the unpredictable energy surpluses and deficits associated with solar energy. In the next section of this chapter we present the efforts dedicated for designing a hybrid system, which simultaneously features a PV device and at the same time elucidates the prospect of direct solar storage. The design of the system is nurtured from exploiting MOx semiconductors which grant several remarkable functionalities in different electronic fields such as energy storage and solar conversion.

7.2. MOx for solar-supercapacitor application

Typically a key solution to the intermittence issues of the solar conversion systems is addressed by the direct coupling of the system to the energy storage devices such as rechargeable batteries and the supercapacitors. This approach often requires additional power electronics to meet the conversion necessities from the PV cell to the storage device which, normally encompass sever ohmic losses and maintenance. In the attributed research (*not included in the thesis due to patenting confidentiality*), we have exploited a simple design solution based on multifunctional implication of the Co_3O_4 semiconductors, which delve into as a thermodynamically suitable (energy band-gap ~1.5 eV) p-type light

absorber layer in a PV system and simultaneously presents viable intrinsic capacitance properties for storage devices. In our dedicated hybrid device, we were required to put front a suitable design solution which permits the Co_3O_4 function as photo-absorber layer and also provides the kinetics for ion absorption and desorption process with enough active surface area for capacitance retention. In that sense, we have fabricated a direct p-n heterojunction solely based on MOx semiconductors, of which the p-type absorber layer, is composed of NRs geometry of Co_3O_4 (Figure 23). Subsequently, the heterojunction structure was interfaced with ionic electrolyte which couples the structure to a counter electrode with comparable ion storage intrinsic capacitance and conductivity for carrier collection.

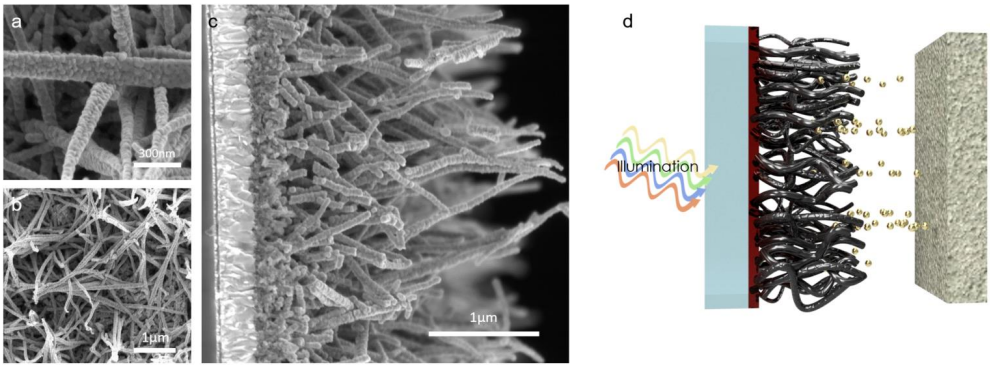

Figure 23: (a)-(c) SEM images of the fabricated nanostructured MOx heterojunction. The NRs geometry of the Co_3O_4 was grown on n-type electron donor layer of Fe_2O_3. (d) The schematic illustration of the designed solar-supercapacitor hybrid device.

The morphological details of the fabricated solar supercapacitor (SSC) device are shown in Figure 23 (d). The illumination direction of the operating device is held from the conductive fluorinated doped tin oxide (FTO) glass substrate towards the heterojunction. Further we have characterized the PV performance of the heterojunction, probing the *J-V* curves of the cell in dark conditions and under 1.5 AM Sun illumination. The bare nanostructured heterojunctions delivered a moderate V_{oc} values of 0.24±0.03 V and J_{sc} of $(5.1\pm0.2)\times10^{-3}$ mA under illumination. We have assigned the relatively low PV values to the possible space chare regions effect created in the NRs geometry and the difficulties in retiring the current from the high surface area of the samples. On the other hand, the PV performance of the hybrid devices, after integration as a SSC, were drastically increased

(Figure 24 (c)). We have reported the average V_{oc} values of 0.6±0.2 V for the device in the full-charge state and the beginning of illuminations. Here, the increase in the open circuit potential and the derived current can be assigned to the two simultaneous processes of PV effect in the heterojunction device and the excess delivered charges to the electrodes from the accumulated Li^+ ions on the electrodes.

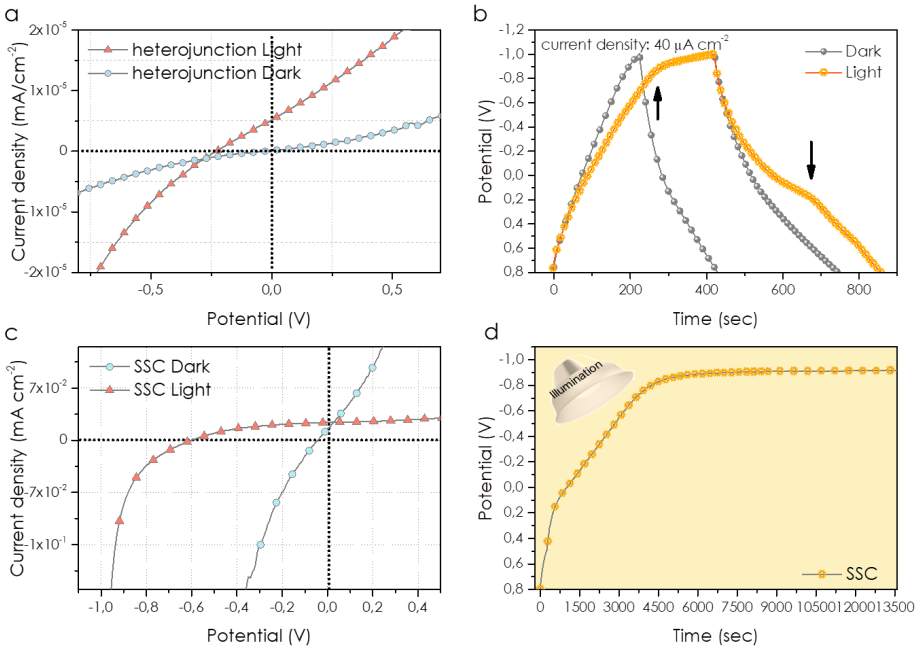

Figure 24: The J-V characteristic of the fabricated sample before (a) and after (c) intervention of the carrier storage abilities to the device. (b) Charge- discharge curves of the sample in dark and under 1.5 AM illuminations. (d) Photo-charging the SSC device only with Sun illumination and no applied bias potential.

The charge and discharge characteristics of the SSC devices shown in Figure 24(b),(d) demonstrated the pseudo-capacitive behavior of the samples in the dark conditions. Two clear plateaus were observed in the charge and discharge curves of the SSC under illumination, one where the charging potential of the samples surpasses the V_{oc} of the constituent heterojunctions (around -0.81 V) and another one where the discharge curve inclines toward the positive potential. We have assigned the first plateau to the tendency

of the SSC devices to uphold the V_{oc} values of the original PV cell. Subsequently, increasing the potential after -0.82 V is proceeded with a much slower rate (from -0.82 to -1 V). The second plateau where the discharging potential tends toward the positive region, presents a broad shoulder and a slower decay of the curve. This phenomenon is attributed to the tendency of the SSC device to be in the negative potential under illumination. We have probed the storage capacity of the SSC devices only with 1.5 AM irradiation, and no applied bias. Remarkably, the device architecture permits the ion storage kinetic transitions from the complete discharge state (0.8 V) to complete charging state (-1 V) via solar excitation. Correspondingly, the plateau of the photo-charging in the devices presents a slower trend for potential rise-time above the open circuit potential limit of the constituent PV cell. Overall we have estimated the photo-charge time frame of around 98 minutes for the system to reach 90% of its total charging capacity.

CHAPTER 8

Conclusions

The MOx based optoelectronic devices have seen tremendous advances during the last years. The enticing light-matter interaction and the prospect of their ion storage abilities of their consequent systems enables for a new and high performance class of devices.

The combination of wide and facile spectral tunability, remarkable absorption cross-section, abundance, and intrinsic capacitance is especially appealing for photovoltaic, sensing and energy storage applications. The results presented in this thesis aim at representing an advance in the knowledge and performance of the MOx in variety of technologies.

Significant challenges existed nevertheless prior to this work, which posed severe restrictions to the potential of this optoelectronic platform, both from performance and implementation perspectives. In this thesis, we have addressed the aforementioned issues and aimed for resolving the prospect of challenges with our research findings.

Demonstration of light-trapping in MOx based heterojunction solar cell

Prior to this thesis, one of the major roadblocks to make MOx based heterojunction PV devices deployable, was the lack of a p-type MOx platform that, while being compatible with large-scale manufacturing processes, would give access to sufficient photogenerated current, and at the same time preventing significant light loss. In the first part of this thesis the light harvesting 1D structures of Co_3O_4 NRs forest have been discussed, suggesting an original approach to successfully increase the light absorption properties of the subsequent heterojunctions through internal light-scattering. Moreover, the PV properties of these material have been studied, in order to give deeper insight on the photoexcited carrier generation/transport, of the consequent PV devices.

Spectral response and carrier transfer dynamics in plasmonic Schottky systems

The most straightforward approach to harvest plasmonic hot-electrons is the Schottky metal-semiconductor junction. In this thesis we identified the crucial role of the interface engineering and the hot-carrier plasmonic transfer processes of the noble metals to semiconductors due to coupling with electromagnetic optical field. In chapter 4 we pinpointed different mechanism of hot-carrier injection in the plasmonic silver and ZnO NRs junction. In doing so, we successfully distinguished the two competing hot-carrier transfer mechanism of Ag NPs and ZnO NRs, using a thin intermediate insulating layer of Al_2O_3 which enabled for tuning the injection mechanism. Using ultrafast transient pump-probe spectroscopy and targeted photoresponse of the system we monitored the role of dipole-dipole hot carrier transfer mechanism and Fawler-Nordheim tunneling process in the spectral response of the ZnO NRs.

In-depth photoexcited carrier transfer in MOx semiconductor

In chapter 5 we introduced a first time reported use of vertically aligned scaffold of graphene in order to mediate the photoexcited carrier transfer in MOx semiconductors. We relied on several facile manufacturing techniques for fabrication of the devices which can ultimately be applicable for the future studies of these junctions. Using intermodulation conductive force microscopy, we managed to monitor the carrier-carrier scattering mechanism of rGO network mediating the in-depth photoexcited carrier transfer in adjacent MOx semiconductor. Within this context, we have fabricated an all-oxide heterojunction device, based on the rGO integrated MOx composite, providing the first proof of concept in which the carrier-carrier relaxation pathways of integrated rGO can facilitate the conversion process of the consequent PV device.

Direct solar energy storage

The final part of this thesis focused on the fabrication of a first time reported energy storage device, providing the possibilities to harvest and store the photo-converted carriers. We thoroughly investigate the operating mechanisms of the hybrid device, and determined the suitable operating conditions. Catering the novel design of the SSC device we have provided a guideline for ample carrier collection of the MOx heterojunction PVs, and simultaneously stabilized the output power of the system. We believe that the

reported device will play an important role in the development of new systems for a more efficient and widespread exploitation of renewable energies.

To conclude, we expect the dedicated work presented here to mean a significant milestone towards a new generation of devices with enhanced functionalities beyond classical semiconductor limits and can be considered as a paved way for optoelectronic applications.

Bibliography

[1] European Renewable Energy Council, *Renewable Energy in Europe*; Routledge, 2010.

[2] S. Aggarwal, N. Kumar, In *Advances in Computers*; 2021; Vol. 121, pp. 455–481.

[3] A. F. Zobaa, R. C. Bansal, *HANDBOOK OF RENEWABLE ENERGY TECHNOLOGY*; World Scientific Publishing Co. Pte. Ltd., 2011.

[4] S. E. Utilization, *Solar Energy Utilization: Fundamentals and Aplicatios*; 1986.

[5] F. H. Alharbi, S. Kais, *Renew. Sustain. Energy Rev.* **2015**, *43*, 1073.

[6] A. Datas, C. Algora, *Prog. Photovoltaics Res. Appl.* **2012**, *21*, n/a.

[7] M. A. Green, E. D. Dunlop, J. Hohl-Ebinger, M. Yoshita, N. Kopidakis, X. Hao, *Prog. Photovoltaics Res. Appl.* **2021**, *29*, 657.

[8] J. Jean, P. R. Brown, R. L. Jaffe, T. Buonassisi, V. Bulović, *Energy Environ. Sci.* **2015**, *8*, 1200.

[9] B. E. Conway, B. E. Conway, In *Electrochemical Supercapacitors*; Springer US: Boston, MA, 1999; pp. 11–31.

[10] B. E. Conway, In *Electrochemical Supercapacitors*; Springer US: Boston, MA, 1999; pp. 33–65.

[11] J. Chmiola, *Science (80-.).* **2006**, *313*, 1760.

[12] M. A. Green, Commercial progress and challenges for photovoltaics. *Nat. Energy* **2016**, *1*, 15015.

[13] A. Richter, M. Hermle, S. W. Glunz, *IEEE J. Photovoltaics* **2013**, *3*, 1184.

[14] M. A. Green, In *McEvoy's Handbook of Photovoltaics*; Elsevier, 2018; pp. 95–128.

[15] M. a. Green, **1995**, 366.

[16] W. Shockley, H. J. Queisser, *J. Appl. Phys.* **1961**, *32*, 510.

[17] B. K. Ghosh, C. N. J. Weoi, A. Islam, S. K. Ghosh, *Renew. Sustain. Energy Rev.* **2018**, *82*, 1990.

[18] M. A. Green, *Phys. E Low-dimensional Syst. Nanostructures* **2002**, *14*, 65.

[19] J. Iqbal, L. Li, A. Numan, S. Rafique, R. Jafer, S. Mohamad, M. Khalid, K. Ramesh, S. Ramesh, *New J. Chem.* **2019**, *43*, 13183.

[20] Q. Li, S. Zheng, Y. Xu, H. Xue, H. Pang, *Chem. Eng. J.* **2018**, *333*, 505.

[21] Y. Zhang, Y. Liu, J. Chen, Q. Guo, T. Wang, H. Pang, *Sci. Rep.* **2014**, *4*, 2.

[22] Y. Hu, Y. Wu, J. Wang, *Adv. Mater.* **2018**, *30*, 1.

[23] T. Deng, W. Zhang, O. Arcelus, J. G. Kim, J. Carrasco, S. J. Yoo, W. Zheng, J. Wang, H. Tian, H. Zhang, X. Cui, T. Rojo, *Nat. Commun.* **2017**, *8*.

[24] H. Y. Lee, J. B. Goodenough, *J. Solid State Chem.* **1999**, *223*, 220.

[25] P. Ghamgosar, F. Rigoni, S. You, I. Dobryden, M. G. Kohan, A. L. Pellegrino, I. Concina, N. Almqvist, G. Malandrino, A. Vomiero, *Nano Energy* **2018**, *51*, 308.

[26] T. Minami, Y. Nishi, T. Miyata, *Appl. Phys. Express* **2015**, *8*, 022301.

[27] P. Ghamgosar, F. Rigoni, M. G. Kohan, S. You, E. A. Morales, R. Mazzaro, V. Morandi, N. Almqvist, I. Concina, A. Vomiero, *ACS Appl. Mater. Interfaces* **2019**, *11*, 23454.

[28] B. Kupfer, K. Majhi, D. A. Keller, Y. Bouhadana, S. Rühle, H. N. Barad, A. Y. Anderson, A. Zaban, *Adv. Energy Mater.* **2015**, *5*, 1401007.

[29] S. Masudy-Panah, G. K. Dalapati, K. Radhakrishnan, A. Kumar, H. R. Tan, E. Naveen Kumar, C. Vijila, C. C. Tan, D. Chi, *Prog. Photovoltaics Res. Appl.* **2015**, *23*, 637.

[30] S. Rühle, A. Y. Anderson, H.-N. Barad, B. Kupfer, Y. Bouhadana, E. Rosh-Hodesh, A. Zaban, *J. Phys. Chem. Lett.* **2012**, *3*, 3755.

[31] L. Qiao, H. Y. Xiao, H. M. Meyer, J. N. Sun, C. M. Rouleau, A. A. Puretzky, D. B. Geohegan, I. N. Ivanov, M. Yoon, W. J. Weber, M. D. Biegalski, *J. Mater. Chem. C*

2013, *1*, 4628.

[32] S. Masudy-Panah, K. Radhakrishnan, H. R. Tan, R. Yi, T. I. Wong, G. K. Dalapati, *Sol. Energy Mater. Sol. Cells* **2015**, *140*, 266.

[33] G. Hautier, A. Miglio, G. Ceder, G.-M. Rignanese, X. Gonze, *Nat. Commun.* **2013**, *4*, 2292.

[34] M. Gilzad Kohan, G. Solomon, S. You, K. Yusupov, I. Concina, A. Vomiero, *Nano Sel.* **2021**, nano. 202000252.

[35] N. Storey, Storey, Electronics: A Systems Approach, 6th Edition | Pearson.

[36] H. S. Yoon, J. Oh, J. Y. Park, J. S. Kang, J. Kwon, T. Cusati, G. Fiori, G. Iannaccone, A. Fortunelli, V. O. Ozcelik, G. H. Lee, T. Low, S. C. Jun, *NPG Asia Mater.* **2019**, *11*.

[37] C.-Z. Ning, L. Dou, P. Yang, *Nat. Rev. Mater.* **2017**, *2*, 17070.

[38] B. D. Yuhas, P. Yang, *J. Am. Chem. Soc.* **2009**, *131*, 3756.

[39] P. Barthelemy, J. Bertolotti, D. S. Wiersma, *Nature* **2008**, *453*, 495.

[40] J. B. Baxter, E. S. Aydil, *Appl. Phys. Lett.* **2005**, *86*, 1.

[41] A. Lagendijk, B. van Tiggelen, D. S. Wiersma, *Phys. Today* **2009**, *62*, 24.

[42] P. Barthelemy, J. Bertolotti, D. S. Wiersma, *Nature* **2008**, *453*, 495.

[43] C. Clavero, *Nat. Photonics* **2014**, *8*, 95.

[44] F. P. García de Arquer, A. Mihi, D. Kufer, G. Konstantatos, *ACS Nano* **2013**, *7*, 3581.

[45] H. A. Atwater, A. Polman, *Nat. Mater.* **2010**, *9*, 205.

[46] G. Qiu, Z. Gai, Y. Tao, J. Schmitt, G. A. Kullak-Ublick, J. Wang, *ACS Nano* **2020**, *14*, 5268.

[47] A. G. Brolo, *Nat. Photonics* **2012**, *6*, 709.

[48] M. Xiao, R. Jiang, F. Wang, C. Fang, J. Wang, J. C. Yu, *J. Mater. Chem. A* **2013**, *1*, 5790.

[49] X.-C. Ma, Y. Dai, L. Yu, B.-B. Huang, *Light Sci. Appl.* **2016**, *5*, e16017.

[50] S. Mubeen, J. Lee, W. Lee, N. Singh, G. D. Stucky, M. Moskovits, *ACS Nano* **2014**, *8*, 6066.

[51] P. Sensitivity, In *Encyclopedia of Neuroscience*; Springer Berlin Heidelberg: Berlin, Heidelberg, 2008; Vol. 107, pp. 1060–1060.

[52] S. Link, M. A. El-Sayed, *Int. Rev. Phys. Chem.* **2000**, *19*, 409.

[53] G. Zhao, H. Kozuka, T. Yoko, *Thin Solid Films* **1996**, *277*, 147.

[54] Y. Tian, T. Tatsuma, *Chem. Commun.* **2004**, 1810.

[55] T. Kawawaki, Y. Takahashi, T. Tatsuma, *Nanoscale* **2011**, *3*, 2865.

[56] S. D. Standridge, G. C. Schatz, J. T. Hupp, *J. Am. Chem. Soc.* **2009**, *131*, 8407.

[57] P. Reineck, G. P. Lee, D. Brick, M. Karg, P. Mulvaney, U. Bach, *Adv. Mater.* **2012**, *24*, 4750.

[58] M. A. Mahmoud, M. Chamanzar, A. Adibi, M. A. El-Sayed, *J. Am. Chem. Soc.* **2012**, *134*, 6434.

[59] C. Burda, X. Chen, R. Narayanan, M. A. El-Sayed, *Chem. Rev.* **2005**, *105*, 1025.

[60] X. Ma, Y. Dai, L. Yu, Z. Lou, B. Huang, M.-H. Whangbo, *J. Phys. Chem. C* **2014**, *118*, 12133.

[61] S. K. Cushing, J. Li, F. Meng, T. R. Senty, S. Suri, M. Zhi, M. Li, A. D. Bristow, N. Wu, *J. Am. Chem. Soc.* **2012**, *134*, 15033.

[62] S. K. Behura, C. Wang, Y. Wen, V. Berry, *Nat. Photonics* **2019**, *13*, 312.

[63] S. Tongay, T. Schumann, X. Miao, B. R. Appleton, A. F. Hebard, *Carbon N. Y.* **2011**, *49*, 2033.

[64] C.-C. Chen, M. Aykol, C.-C. Chang, A. F. J. Levi, S. B. Cronin, *Nano Lett.* **2011**, *11*, 1863.

[65] H. Zhong, Z. Liu, G. Xu, Y. Fan, J. Wang, X. Zhang, L. Liu, K. Xu, H. Yang, *Appl. Phys. Lett.* **2012**, *100*, 122108.

[66] T. Oka, H. Aoki, *Phys. Rev. B* **2009**, *79*, 081406.

[67] R. Ifuku, K. Nagashio, T. Nishimura, A. Toriumi, *Appl. Phys. Lett.* **2013**, *103*, 033514.

[68] R. Bistritzer, A. H. MacDonald, *Phys. Rev. Lett.* **2009**, *102*, 206410.

[69] R. Kim, V. Perebeinos, P. Avouris, *Phys. Rev. B* **2011**, *84*, 075449.

[70] M. K. L. Man, J. Madéo, C. Sahoo, K. Xie, M. Campbell, V. Pareek, A. Karmakar, E. L. Wong, A. Al-Mahboob, N. S. Chan, D. R. Bacon, X. Zhu, M. M. M. Abdelrasoul, X. Li, T. F. Heinz, F. H. da Jornada, T. Cao, K. M. Dani, *Sci. Adv.* **2021**, *7*, eabg0192.

[71] F. Xia, T. Mueller, Y. Lin, A. Valdes-Garcia, P. Avouris, *Nat. Nanotechnol.* **2009**, *4*, 839.

[72] A. Yamakage, K.-I. Imura, J. Cayssol, Y. Kuramoto, In *AIP Conference Proceedings*; 2012; Vol. 1504, pp. 867–870.

[73] G. Rao, M. Freitag, H.-Y. Chiu, R. S. Sundaram, P. Avouris, *ACS Nano* **2011**, *5*, 5848.

[74] F. Vaianella, G. Rosolen, B. Maes, *J. Appl. Phys.* **2015**, *117*.

[75] J. P. Shim, M. Choe, S. R. Jeon, D. Seo, T. Lee, D. S. Lee, *Appl. Phys. Express* **2011**, *4*, 4.

[76] L. Kavan, J. H. Yum, M. Grätzel, *ACS Nano* **2011**, *5*, 165.

[77] Q. D. Yang, J. Li, Y. Cheng, H. W. Li, Z. Guan, B. Yu, S. W. Tsang, *J. Mater. Chem. A* **2017**, *5*, 9852.

[78] K. Majhi, L. Bertoluzzi, D. A. Keller, H.-N. Barad, A. Ginsburg, A. Y. Anderson, R. Vidal, P. Lopez-Varo, I. Mora-Sero, J. Bisquert, A. Zaban, *J. Phys. Chem. C* **2016**, *120*, 9053.

[79] M. Gilzad Kohan, R. Mazzaro, V. Morandi, S. You, I. Concina, A. Vomiero, *J. Mater. Chem. A* **2019**, *7*, 26302.

Department of Engineering Sciences and Mathematics
Division of Materials Science

ISSN 1402-1544
ISBN 978-91-7790-906-4 (print)
ISBN 978-91-7790-907-1 (pdf)

Luleå University of Technology 2021

Print: Lenanders Grafiska, 137688

LULEÅ UNIVERSITY OF TECHNOLOGY